Journal of South American Earth Sciences 121 (2023) 104135

Contents lists available at ScienceDirect

Journal of South American Earth Sciences

journal homepage: www.elsevier.com/locate/jsames

Groundwater Heat Pump assessment operation in three cities of south-central Chile: An approach based on aquifer characterization and analytical calculations of Thermal Affectation Zone

Mauricio Muñoz *, Diego Aravena, Karin García, Nicolás Hurtado, Esteban Micco, Diego Morata

Centro de Excelencia en Geotermia de los Andes (CEGA), Facultad de Ciencias Físicas y Matemáticas, Universidad de Chile, Santiago, Chile
Departamento de Geología, Facultad de Ciencias Físicas y Matemáticas, Universidad de Chile, Santiago, Chile

ARTICLE INFO

Keywords:
Groundwater Heat Pump (GWHP)
South central Chile
Hydraulic parameters of the aquifer
Thermal Affectation Zone (TAZ)

ABSTRACT

The aim of this work is the Groundwater Heat Pump (GWHP) assessment in three cities in south central Chile (Talca, Temuco, and Osorno), considering the hydraulic parameters of the aquifer, its temperature, and the Thermal Affectation Zone (TAZ) generated around the reinjection well due to the reinjected water flow, and temperature difference, due to thermal recovery.

According to the hydraulic characterization, the conditions are more favorable in the city of Talca, where the hydraulic conductivity is medium to high. On the other hand, in the cities of Temuco and Osorno, the hydraulic conductivity is low or very low, except in some domains of river belts, where the hydraulic conductivity is medium to high. In all cities, the temperature of the aquifer is very good for heating and cooling. In particular, in Talca downtown there is a positive thermal anomaly that improves the GWHP performance for heating purposes.

In each city, the extension of the TAZ was calculated for a reinjection rate of 5 [L/s], and a thermal recovery of 3 [°C] (heating). In each city, the TAZ was calculated for the hydraulic conductivity values corresponding to the percentiles 25, 50, and 75. The hydraulic gradient is fixed for each city. The heating time increases from north to south (Talca, Temuco and Osorno) due to the climate. In all cities and in all cases, temperature dispersion due to groundwater flow is moderate to slight and concentrated around the reinjection well. The largest extension of TAZ in the direction of groundwater flow is calculated in Talca, reaching approximately 30 m. On the other hand, the greatest reach of TAZ in the opposite direction to the groundwater flow is calculated in Osorno, reaching approximately 20 m. The effect of varying injection rates (3, 5 and 10 L/s) does not significantly affect the distance range of TAZ, yet affects the concentration of TAZ around the reinjection well.

1. Introduction

The IPCC's Sixth Assessment Report warns that climate change is widespread, rapid, and intensifying. From 1850–1900 to date, the global temperatures have increased by 1.1 °C, affecting billions of people worldwide. To mitigate this trend, it is mandatory to replace the use of fossil fuels with efficient heating and cooling technologies such as the Geothermal Heat Pump (GHP).

The GHP is a mature technology in Asia, Europe, and North America (Lund and Toth, 2021). Conversely, the use of GHP is growing at a slower rate in South América. For instance, in Chile there are about 70 GHP documented, which account for 8.6 MWth (Morata et al., 2020) The open cycle is the most frequent ground source heat exchanger (45%) i.e., most of the installations correspond to Groundwater Heat Pump (GWHP) (Morata et al., 2020). In recent years, there has been an increase in companies installing GHP. Nevertheless, installation costs are still high, consistent with the unconsolidated market.

A heat pump (HP) 'moves' heat from a lower-temperature source to a higher-temperature sink. A GWHP consists of a water-to-water HP coupled to an array of wells for extracting and reinjecting groundwater. The HP recovers heat from the groundwater (heating) or dissipates heat into the groundwater (cooling), and the groundwater exchanges heat with the ground (Chiasson, 2016; Mustafa Omer, 2008; Banks,

* Corresponding author at: Centro de Excelencia en Geotermia de los Andes (CEGA), Facultad de Ciencias Físicas y Matemáticas, Universidad de Chile, Santiago, Chile.
E-mail address: maumunoz@uchile.cl (M. Muñoz).
URL: https://www.cega-uchile.cl (M. Muñoz).

https://doi.org/10.1016/j.jsames.2022.104135
Received 6 July 2022; Received in revised form 14 October 2022; Accepted 23 November 2022
Available online 26 November 2022
0895-9811/

2012). The relatively stable temperature of the groundwater yields a higher efficiency than air-source heat pump systems, thus a productive and shallow aquifer usually favors the GWHP functioning (Clauser, 1997; Sanner et al., 2003; Marcic, 2004; Florides and Kalogirou, 2007; Milenić et al., 2010). Therefore, a good stratigraphic, hydrogeological, and temperature record of shallow aquifers allow an accurate GWHP design (Lee and Hahn, 2006; Lo Russo et al., 2012; Wu et al., 2015).

The continuous increase in open loop systems in urban areas can have an effect on underground temperature. The reinjection of cooler water could cause a significant subsurface impact leading to local variations in groundwater temperature within the Thermally Affected Zone (TAZ) that develops around the reinjection well (Banks, 2009; Lo Russo et al., 2012). The extension of the TAZ must be well predicted and constantly controlled in order to guarantee the systems' long-term sustainable use (e.g., Gizzi et al., 2020). Therefore, several analytical solutions for continuous injection of heat into a uniform flow field have been developed (Fetter, 1999; Metzger et al., 2004; Banks, 2011; Chiasson, 2016).

This study presents a database of stratigraphy, hydraulic parameters and groundwater temperature in Talca, Temuco and Osorno cities, located in south-central Chile. The collected data are used as initial and boundary conditions to calculate the TAZ with an analytical solution after Chiasson (2016). The TAZ is calculated for the operation in heating mode of the GWHP, since it is the main thermal requirement in the cities of interest. It is expected that further exploration of shallow geothermal resources will support an accurate design of GWHP in the Chilean geological context, helping to achieve the country's ambitious goals of access to thermal comfort and particulate matter reduction emissions (Huneeus et al., 2020).

2. Geological and climatic setting

The main features of the geological setting of Talca, Temuco and Osorno cities (Fig. 1) are described below.

The Talca city in central Chile (35.4° S), is located in the central valley between the Coastal Range to the west and the Main Andean Range to the east. The rocks of the eastern flank of the Coastal Range constitute the rock basement. These rocks correspond to volcanic and volcano-sedimentary rocks from the Cretaceous (Cv). The volcanic rocks are composed of stratified tuffs and breccias with interbedded porphyritic lavas. This well-bedded volcanic-sedimentary sequence is intruded by Early Cretaceous granodiorites (Cg) (Bravo, 2001) (Fig. 1.b). The sedimentary infill of Talca city is composed of Holocene fluvio-alluvial and fluvial deposits (Qf). Furthermore, Quaternary pyroclastic deposits cover a large area of the city (Qv) (Fig. 1.b). These pyroclastic deposits can also be found interbedded within the clastic sedimentary non-consolidated sequence (Hauser, 1995).

The Temuco city in central Chile (38.7° S), is located in the central valley, between the Coastal Range to the west and the Main Andean Range to the east. The basement rocks correspond to Oligocene sedimentary and volcanic rocks (Ovs) (Fig. 1.c). The sedimentary sequence comprises sandstones, siltstones, and shales. There are andesites and tuffs interbedded within the clastic sedimentary sequence. These volcanic rocks predominate in the upper part. This stratified sequence is intruded by subvolcanic bodies (Mella and Quiroz, 2010). The sedimentary infill is composed of Pliocene to Pleistocene alluvial (Pa), partially consolidated glacier (Qg), and Holocene fluvial sediments (Qf) (Fig. 1.c). There are also pyroclastic layers interbedded within the clastic sedimentary non-consolidated sequence (Rubio, 1990).

The Osorno city in central southern Chile (40.6° S), is located in the central valley, between the Coastal Range to the west and the Main Andean Range to the east. The rocks of the eastern flank of the Coastal Range constitute the rock basement, comprising Miocene marine sedimentary sequences. The sedimentary infill of the city of Osorno is composed of glacial (Qg), fluvioglacial (Qfg), and fluvial sediments (Qf) (Fig. 1.d). Furthermore, Quaternary pyroclastic deposits cover a large area of the city (Qv) (Fig. 1.d). These pyroclastic deposits can also be found interbedded within the clastic sedimentary non-consolidated sequence (Pérez et al., 2003).

In Continental Chile there are three first-order climates: arid, temperate, and polar. These climates are distributed from north to south and modulated by the elevation of the Andes. In the central zone of Chile, where Talca and Temuco are located, the Mediterranean climate predominates (Sarricolea et al., 2017). In Talca the mean annual temperature is 13.8 °C, ranging from 3.9 °C in winter to 29.7 °C in summer (Santibáñez Quezada, 2017a). In Temuco the mean annual temperature is 12 °C ranging from 3.8 °C in winter to 25 °C in summer (Santibáñez Quezada, 2017b). In central southern Chile, where Osorno is located, the Marine West Coast climate predominates (Sarricolea et al., 2017). In Osorno the annual mean temperature is 11 °C ranging from 3.2 °C in winter to 22.8 °C in summer (Santibáñez Quezada, 2017c). This climatic context is later used to determine the operating time in heating mode of the geothermal facilities in each of the cities of interest.

3. Data availability

The pumping tests and the stratigraphic records were collected from the database of the General Directorate of Waters of Chile (Dirección General de Aguas, DGA). For this work, 123 wells located in, or around urban areas were selected considering the quality of the information. There are many more wells in the DGA database, but with lower quality data or incomplete information. For practical purposes, the wells were labeled from 1 to 123 (the correlation with the DGA code can be reviewed in the Supplementary data). The considerations to generate the database and the data treatment are described below.

3.1. Stratigraphic description

The stratigraphic information, from the DGA database, is standardized considering sedimentary environment during deposition (e.g., Fig. 2). In addition, the calculated hydraulic properties allow us to verify if the sedimentary deposits are consistent, because these properties depend on the type of sediment (Custodio and Llamas, 1996).

As will be seen later, the stratigraphic columns are used to draw stratigraphic cross sections, which allow to visualize the extension and thickness of the unconsolidated sedimentary layers. In most cases, the layers were grouped into larger geological units to simplify information and allow comparison.

3.2. Features of well construction

There is record of the well construction features in most of the cases. Here it is considered well depth, casing diameter and screen length (e.g., Fig. 2). These records, together with the pumping test record, are input data for hydraulic properties calculation. The Tables 1, 3, and 5 summarize the construction data of the wells considered in the cities of Talca, Temuco and Osorno, respectively.

3.3. Temperature of groundwater

Temperature profiles were measured inside wells during 2012 (Talca), 2016 (Temuco), and 2017 (Osorno) (Tables 2, 4, and 6). All measurements were made in wells drilled at least several months ago and inactive before taking the measurements, so there are no temperature disturbances due to drilling or groundwater pumping. The temperature record in the wells was discrete every one meter (e.g., Fig. 2), thus avoiding effects related to convection cells, which are usually on the order of one meter in height (Beardsmore and Cull, 2001). In the city of Talca, the Antares 1854 probe was used (accuracy of ±0.1 °C). In the cities of Temuco and Osorno, the TLC probe model 107 was used (accuracy of ±0.2 °C).

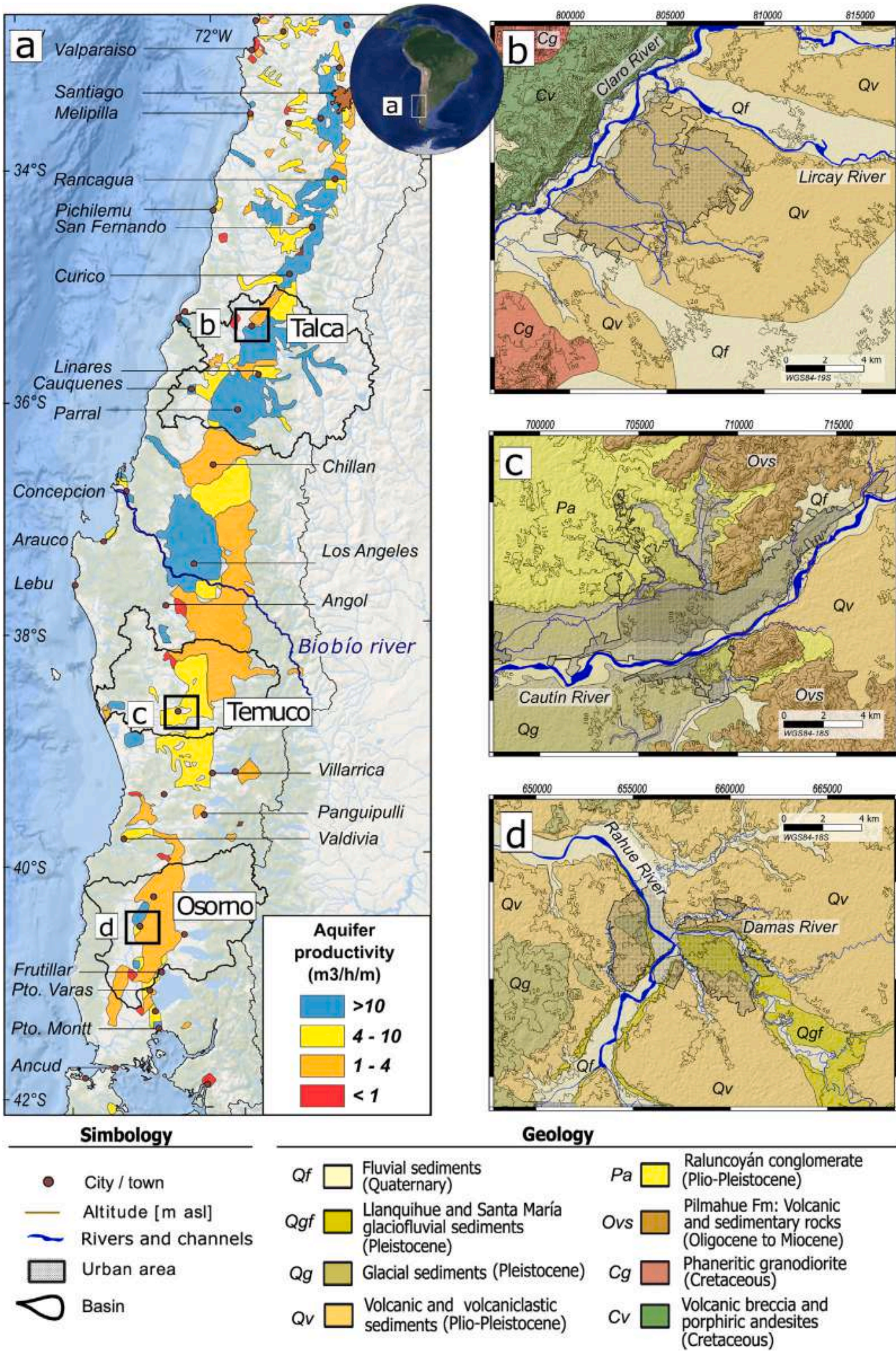

Fig. 1. (a) Location of selected cities and aquifer productivity in south-central Chile (productivity modified after DGA, 1986). Geology, main rivers, and urban areas in the cities of (b) Talca (modified after Varela and Moreno, 1982; Hauser, 1995; Bravo, 2001), (c) Temuco (modified after Mella and Quiroz, 2010), and (d) Osorno (modified after Pérez et al., 2003).

According to Beardsmore and Cull (2001), the magnitude of the temperature perturbation in depth due to variation in surface temperature is given by one effective wavelength (z_{wl}) calculated as follows:

$$z_{wl} = (4\pi P k)^{\frac{1}{2}} \quad (1)$$

Here, P is the period of time in seconds [s], k is thermal diffusivity [$m^2 s^{-1}$].

For the seasonal cycle the period of the temperature perturbation is one year, P = 3.1557×10^7 s. According to average thermal diffusivity value of 1.1×10^{-6} in case of Talca (mainly composed of saturated sand

Table 1
Collected hydrogeological data and calculated hydraulic parameters in the city of Talca.

ID	UTM E m	UTM N m	Depth m	DWL m	Date DD/MM/YY	Flow rate L/s	H. conductivity m/day	Transmissivity m^2/day	Aquifer thickness m	Ash/tuff
1	263,384	6,081,051	80.0	0.0	12/09/02	90.0	25.92	2073.6	80.0	No
2	262,973	6,080,808	46.2	8.0	05/10/14	25.0	1.47	68.3	38.2	No
3	262,146	6,080,603	40.0	8.0	28/08/99	20.0	15.55	578.9	32.0	No
4	260,112	6,078,492	28.0	8.8	24/06/14	3.0	5.88	112.3	19.2	Yes
5	262,720	6,078,176	81.0	15.2	11/11/16	66.0	8.64	570.2	65.8	No
6	262,457	6,078,070	60.0	11.8	22/05/09	30.0	2.59	129.6	48.2	No
7	259,782	6,077,847	16.5	3.7	24/06/14	0.8	1.73	22.5	12.8	No
8	261,266	6,077,583	73.0	5.1	11/07/08	28.0	0.21	13.8	68.0	No
9	257,728	6,077,470	48.5	9.7	07/04/06	5.0	–	–	38.8	Yes
10	255,278	6,077,280	12.2	3.7	22/07/15	3.2	6.39	53.6	8.5	No
11	257,366	6,077,218	67.0	0.0	28/04/07	8.4	5.88	388.8	67.9	No
12	263,570	6,076,995	43.7	14.5	11/09/04	13.5	7.34	216.0	29.2	No
13	260,711	6,076,786	35	3.8	02/10/05	14.9	4.84	155.5	31.2	No
14	259,967	6,076,781	18.0	4.0	30/09/14	3.3	17.28	241.9	14.0	No
15	261,673	6,076,637	50.0	12.7	02/12/16	40.0	82.94	3110.4	37.3	No
16	259,372	6,076,341	80.0	4.9	20/12/12	50.0	7.00	527.0	75.1	No
17	263,478	6,076,183	25.0	11.8	22/02/11	5.3	10.37	138.2	13.2	No
18	263,170	6,075,359	16.0	3.3	11/04/16	3.0	8.29	103.7	12.7	No
19	262,103	6,074,574	65.0	15.1	11/11/06	26.0	28.51	1382.4	49.9	No
20	263,982	6,073,575	30.0	10.8	08/05/18	4.0	13.82	267.8	19.2	No
21	263,935	6,073,528	30.0	4.3	08/05/18	4.3	14.69	276.5	25.7	No
22	259,839	6,072,032	30.0	2.8	01/04/18	16.0	2.07	57.0	27.2	No
23	265,170	6,071,128	70.0	11.2	30/01/99	51.0	59.61	3542.4	58.8	No
24	254,663	6,070,414	24.0	7.3	31/01/17	3.2	3.89	64.8	16.7	No
25	268,743	6,070,142	40.0	5.1	21/12/96	5.0	3.37	121.0	34.9	No
26	257,285	6,065,531	45.0	3.0	06/04/11	40.0	0.75	31.1	42.0	Yes

Table 2
Average well temperature measured in Talca in October of 2012.

ID	UTM N m	UTM E m	Temperature °C
T01	6,077,707	257,765	18.4
T02	6,089,847	270,901	17.9
T03	6,085,128	265,932	19.8
T04	6,078,815	260,921	17.6
T05	6,076,268	271,330	16.8
T06	6,060,916	276,552	16.2
T07	6,080,461	262,598	16.7
T08	6,080,001	270,952	17.1
T09	6,081,658	267,200	16.9
T10	6,057,664	265,241	16.9
T11	6,076,538	259,696	18.9
T12	6,076,517	259,647	18.8
T13	6,079,682	277,355	17.0
T14	6,053,577	282,407	15.7
T15	6,070,189	299,730	16.3
T16	6,054,300	251,494	16.9
T17	6,084,795	275,126	17.5
T18	6,086,841	278,573	17.1
T19	6,082,830	264,560	18.3
T20	6,076,933	267,256	16.3
T21	6,069,546	289,465	16.7
T22	6,059,558	254,652	16.1
T23	6,060,185	256,364	17.3
T24	6,048,603	282,509	15.4
T25	6,060,022	279,840	16.2
T26	6,076,942	281,483	16.8
T27	6,069,359	270,402	15.6
T28	6,072,261	266,365	16.3
T29	6,046,592	257,844	16.2
T30	6,056,727	255,773	15.5
T31	6,057,522	253,499	16.5
T32	6,045,277	253,484	17.1
T33	6,081,333	278,689	17.9
T34	6,076,459	259,625	18.5

and gravel), and 0.84×10^{-7} in case of Temuco and Osorno (mainly composed of saturated sand and gravel with silt) (Dalla Santa et al., 2020). The seasonal temperature fluctuation affects up to 20.9 m (Talca) and 18.2 m (Temuco and Osorno). Therefore, only the temperature values measured below 21 m in Talca and below 18 m in Temuco a Osorno are considered. These calculations are conservative because in most cases the shallowest section of the well penetrates dry sediments (with lower thermal diffusivity values), which reduces the depth of surface temperature variation.

In this work, 56 groundwater temperature measurements are considered. Note that temperature monitoring wells did not coincide with the wells where the pumping tests were collected.

3.4. Pumping test and hydraulic conductivity calculation

Hydraulic conductivity is calculated from constant flow pumping tests. Here it is considered tests lasting at least 24 hours (e.g., Fig. 3). In these tests, the recording frequency is higher at the beginning (every minute), and lower to the end (every hour). If the pumping test does not allow hydraulic conductivity calculation, the stratigraphic information is not considered, except in well 9 in Talca, due to its detailed and useful stratigraphic description.

The constant flow pumping test applies a production rate that creates a transient pressure response of the medium, creating a drop in groundwater level, which is analyzed with respect to elapsed time. For the analysis of the pumping tests, the Cooper–Jacob method is used since it can be applied using the pumping well as an observation well. This method determines the transmissivity. Subsequently, from the saturated thickness, the hydraulic conductivity is calculated. The method assumes that the well fully penetrates into the water-saturated medium. Nevertheless, partial penetration as well as losses through the well casing have a minimal effect on the calculations (Halford and Kuniansky, 2002). An example of curve fitting to calculate transmissivity from the pumping test is shown in Fig. 3. The detailed record of each pumping test analysis can be reviewed in the Supplementary material. The Tables 1, 3, and 5 summarize the aquifers features and hydraulic parameters calculated from the wells considered in the cities of Talca, Temuco and Osorno, respectively.

Here, the hydraulic conductivity values are in units of [m/day]. In addition, the calculated values are grouped into ranges considering traditional classifications (e.g., Custodio and Llamas, 1996) and values ranges from spreadsheets generated by the USGS (Halford and Kuniansky, 2002). The hydraulic conductivity values are classified as: high [>9m/day]; medium [<9m/day, >6m/day]; low [<6m/day, >0.9m/day]; and very low [<0.9m/day].

Table 3
Collected hydrogeological data and calculated hydraulic parameters in the city of Temuco.

ID	UTM E m	UTM N m	Depth m	DWL m	Date DD/MM/YY	Flow rate L/s	H. conductivity m/day	Transmissivity m^2/day	Aquifer thickness m	Ash/tuff
27	708,970	5,715,077	21.0	2.1		4.0	0.67	13.0	19.0	No
28	714,820	5,714,784	75.0	6.3	11/09/19	3.6	0.06	4.2	69.0	No
29	707,871	5,714,397	58.0	1.0	23/03/01	5.5	0.13	7.3	57.0	No
30	708,149	5,714,303	46.0	0.9	05/04/01	1.2	0.03	1.2	45.0	No
31	713,831	5,714,270	87.0	37.2	23/05/07	4.5	1.12	54.4	50.0	Yes
32	703,135	5,714,189	61.0	13.8	19/04/19	5.0	0.52	24.2	48.0	No
33	714,165	5,714,041	53.0	8.5	07/06/16	5.5	0.81	36.3	45.0	No
34	713,605	5,713,364	45.0	5.5	22/07/02	3.2	0.05	2.1	40.0	No
35	708,173	5,713,357	70.0	3.8	12/03/99	6.6	0.13	8.6	45.0	No
36	705,088	5,713,205	36.0	14.0	–	3.0	0.54	12.1	22.0	No
37	712,413	5,712,286	30.0	17.3	04/05/98	10.0	8.64	112.3	13.0	No
38	711,659	5,712,243	25.0	3.5	12/07/07	5.5	0.74	16.4	22.0	No
39	705,474	5,709,851	40.0	3.5	24/07/09	8.0	49.25	1641.6	34.0	No
40	707,258	5,709,767	35.0	5.5	02/09/10	24.0	12.10	345.6	30.0	No
41	702,581	5,709,350	32.0	14.0	28/12/12	3.0	2.16	38.9	57.0	No
42	706,810	5,709,297	80.0	15.9	–	12.0	1.30	84.7	64.0	No
43	709,410	5,709,280	30.0	12.8	29/06/09	3.5	0.80	13.8	17.0	No
44	705,001	5,708,969	57.0	6.0	25/07/11	28.0	2.07	103.7	51.0	No
45	705,152	5,708,905	42.0	7.0	19/08/11	36.0	8.04	276.5	35.0	No
46	703,280	5,708,875	27.0	2.0	17/02/18	6.6	0.13	7.3	18.0	No
47	701,613	5,708,786	38.0	2.4	20/03/99	9.8	0.27	9.5	36.0	No
48	709,115	5,708,676	27.0	8.0	22/07/02	8.0	0.67	13.0	19.0	No
49	701,450	5,708,527	30.0	2.2	13/11/10	5.0	1.21	34.6	28.0	No
50	708,764	5,708,460	25.0	5.2	25/02/19	6.8	3.46	68.3	20.0	No
51	701,263	5,708,436	19.0	3.0	25/04/04	5.0	1.38	21.6	16.0	No
52	705,391	5,708,409	120.0	32.3	07/10/15	123.0	8.64	769.0	88.0	Yes
53	706,642	5,708,382	48.3	8.0	09/11/01	8.0	0.84	33.7	40.0	No
54	705,666	5,708,366	62.0	27.4	09/08/06	46.0	3.20	112.3	35.0	No
55	703,710	5,707,922	70.0	14.0	09/08/97	16.2	18.14	1036.8	56.0	Yes
56	709,157	5,707,702	100.0	36.1	17/02/13	35.0	2.76	172.8	64.0	No
57	702,438	5,707,546	21.0	12.0	15/05/00	4.4	31.10	276.5	9.0	No
58	706,623	5,707,431	160.0	14.7	14/05/18	110.0	2.07	302.4	150.0	Yes
59	704,053	5,707,393	30.0	5.7	11/09/03	14.0	1.47	35.4	24.0	No
60	707,927	5,707,279	120.0	19.0	20/12/15	150.0	9.50	1036.8	100.0	No
61	703,894	5,707,040	30.0	7.1	11/02/05	14.0	47.52	1123.2	23.0	No
62	701,775	5,706,748	30.0	2.8	16/09/15	3.0	4.58	121.0	27.0	No
63	704,050	5,706,444	25.0	6.4	29/04/09	3.0	2.76	51.0	19.0	No
64	707,188	5,706,255	57.0	33.1	11/03/16	4.0	2.25	52.7	27.0	No
65	707,667	5,706,193	90.0	35.0	15/02/13	9.0	5.96	328.3	55.0	No
66	707,471	5,706,137	59.0	32.0	15/08/17	4.5	0.45	12.1	27.0	No
67	705,486	5,705,918	52.0	12.0	14/02/12	3.0	0.18	7.1	40.0	No
68	703,435	5,705,401	70.0	30.1	01/11/12	3.6	0.17	6.8	40.0	No
69	704,008	5,705,126	47.0	8.6	20/03/98	4.2	1.04	40.6	38.0	No
70	707,358	5,704,939	30.0	10.9	23/12/10	3.0	0.68	13.0	19.0	No
71	710,243	5,704,784	31.0	4.2	09/03/19	2.0	0.20	5.4	32.0	No
72	706,385	5,704,622	66.0	15.7	24/08/18	30.0	14.69	717.1	53.0	No
73	707,336	5,704,545	46.0	21.5	25/08/18	5.0	2.16	53.6	25.0	No

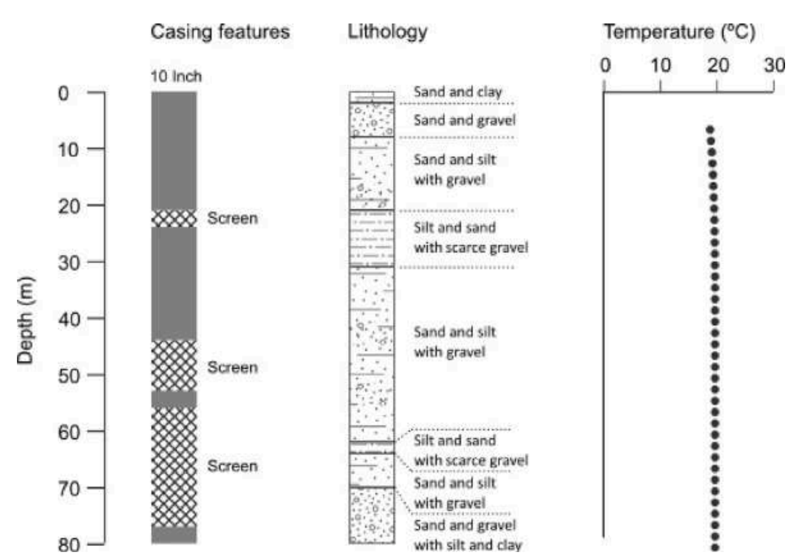

Fig. 2. Example of well construction features, stratigraphic and temperature records in well 16 in the city of Talca.

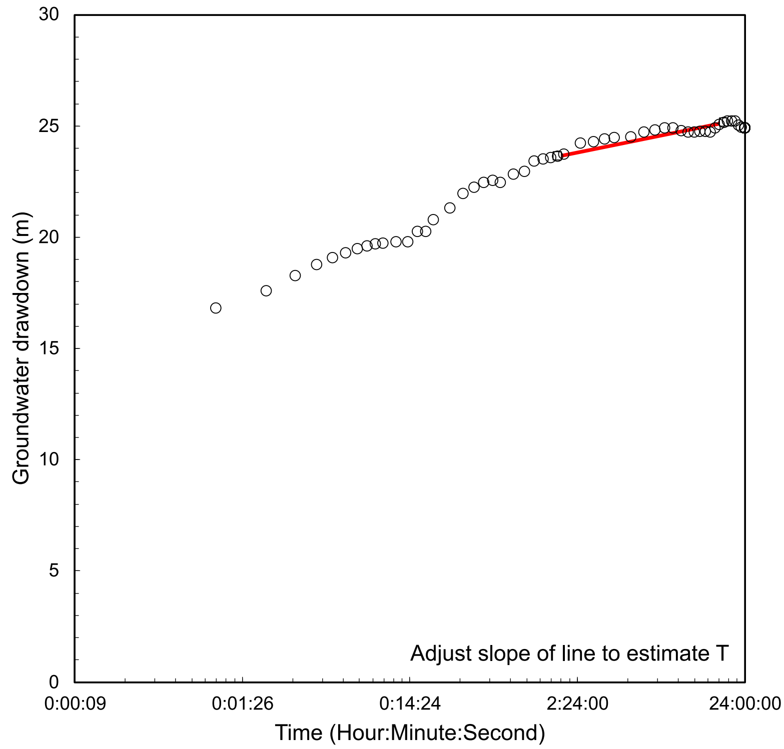

Fig. 3. Example of curve fitting to determine the transmissivity of the aquifer according to the Cooper–Jacob method in well 16 of Talca city. The graph is from Well Test Analysis Spreadsheets (Halford and Kuniansky, 2002). The red line represents the fit to the drawdown curve as a function of time.

Table 4
Average well temperature of selected wells in Temuco in November of 2016.

ID	UTM N m	UTM E m	Temperature °C
Te01	5,711,660	711,880	14.3
Te02	5,711,673	712,388	14.8
Te03	5,711,974	712,787	13.8
Te04	5,712,276	712,904	14.6
Te05	5,708,463	704,349	13.2
Te06	5,707,530	703,846	14.2
Te07	5,707,357	704,935	14.2
Te08	5,707,042	706,302	12.8
Te09	5,707,725	709,132	14.3
Te10	5,707,741	709,082	14.0
Te11	5,709,757	707,260	14.8

4. Methodology: Analytical calculation of TAZ

The method used for the analytical calculation of the thermal affectation zone is after Chiasson (2016). The transportation in groundwater flow can be described by the advection–dispersion equation (Freeze and Cherry, 1979; Bear, 1972). The advection can transport heat by fluid motion through a porous medium. In addition, there is heat dispersion between the fluid and the matrix of the medium, because the groundwater does not flow at the same speed or in the same direction through the medium. This thermal dispersion generates the dissipation of energy in the porous medium.

Applying the energy conservation law in a known volume and using a mass transport analogy for heat transfer, the equation for heat transport in 2D can be expressed as follows:

$$\frac{\partial}{\partial x}\left(D_{xx}\frac{\partial T}{\partial x}\right)+\frac{\partial}{\partial y}\left(D_{yy}\frac{\partial T}{\partial y}\right)-\left(v_x\frac{\partial T}{\partial x}+v_y\frac{\partial T}{\partial y}\right)=R\frac{\partial T}{\partial t} \tag{2}$$

If we consider a homogeneous medium with a uniform velocity, the previous equation for a flow parallel to the x-axis is simplified as follows:

$$D_L\frac{\partial^2 T}{\partial x^2}+D_T\frac{\partial^2 T}{\partial y^2}-v_x\frac{\partial T}{\partial x}=R\frac{\partial T}{\partial t} \tag{3}$$

Here,

$$D_L=a_L v_x+D^* \tag{4a}$$

$$D_T=a_T v_x+D^* \tag{4b}$$

The terms $a_L v_x$ and $a_T v_x$ indicate the dispersion mechanism in longitudinal and transverse directions, respectively. The dispersion values depend on space and time. Xu and Eckstein (1995) developed an empirical relation of longitudinal dispersion (a_L) as a function of the path length traveled by the flow (L) as follows:

$$a_L=0.83\left(\log_{10}(L)\right)^{2.414} \tag{5}$$

The transverse dispersion (a_T) is typically one order of magnitude smaller than a_L. In the mass–energy transport relationship, the diffusion coefficient (D^*) is modeled as the effective thermal diffusivity given by:

$$D^*=\frac{\lambda_{eff}}{\phi\rho_w c_w} \tag{6}$$

Here, λ_{eff} is effective thermal conductivity, ϕ is medium porosity, rho_w is water density, and c_w is water heat capacity.

Considering that heat is stored and conducted by rock and water, yet only advected by water, a retardation coefficient (R) is considered to adjust the advection and diffusion terms (Bear, 1972).

$$R=\frac{(\rho c)_{eff}}{\phi\rho_w c_w} \tag{7}$$

Here, $(\rho c)_{eff}$ is the volumetric heat capacity of the aquifer matrix.

Among the analytical solutions for Eq. (3), the solution of Fetter (1999) is preferred, because it is a solution for a continuous mass injection located at the origin (x,y = (0,0)) into a uniform groundwater flow field with a velocity (v_x) parallel to the x-axis. This solution

Table 5
Collected hydrogeological data and calculated hydraulic parameters in the city of Osorno.

ID	UTM E m	UTM N m	Depth m	DWL m	Date DD/MM/YY	Flow rate L/s	H. conductivity m/day	Transmissivity m^2/day	Aquifer thickness m	Ash/tuff
74	661,093	5,540,583	97.0	24.1	28/10/09	20.0	14.69	1036.8	72.9	No
75	659,803	5,510,261	90.0	29.1	22/12/11	4.0	0.26	16.4	60.9	No
76	660,611	5,509,479	61.0	29.8	12/01/15	5.0	2.76	84.7	31.2	No
77	657,292	5,509,466	144.0	45.4	08/11/16	65.0	1.21	121.0	98.6	No
78	660,592	5,508,713	56.0	12.0	29/02/08	5.4	14.69	639.4	44.0	No
79	659,822	5,508,663	64.0	31.1	02/05/96	33.0	12.10	388.8	32.9	No
80	652,304	5,508,593	33.0	2.0	06/02/15	2.0	0.13	4.1	31.0	No
81	654,074	5,508,101	134.0	60.1	16/11/05	2.0	0.14	10.4	74.0	No
82	661,401	5,507,952	66.0	12.0	04/04/13	5.3	0.95	51.8	54.0	No
83	653,907	5,507,886	87.0	25.6	05/11/15	7.0	0.61	38.0	61.0	No
84	656,901	5,507,837	84.0	26.0	30/08/08	45.0	2.07	121.0	58.0	No
85	661,723	5,507,797	66.0	21.0	29/09/95	3.0	1.12	51.8	45.0	No
86	654,599	5,507,638	128.0	57.8	22/02/16	5.0	0.42	30.2	70.0	No
87	662,308	5,507,633	59.0	25.1	07/06/17	5.0	0.41	13.8	34.0	No
88	658,493	5,507,086	103.0	23.0	18/11/95	40.0	0.64	51.8	81.0	No
89	659,987	5,506,840	54.0	8.4	14/12/00	4.5	3.28	146.9	46.0	No
90	660,878	5,506,572	56.2	3.5	09/10/98	35.0	14.69	786.2	52.7	No
91	660,848	5,506,564	57.0	10.0	01/10/00	15.0	1.30	43.2	32.8	No
92	659,277	5,506,237	60.0	19.0	10/01/16	8.0	3.72	155.5	41.0	No
93	656,929	5,506,081	118.0	3.8	05/08/98	38.0	1.73	190.1	110.0	No
94	661,086	5,506,064	51.0	8.0	13/09/00	31.8	7.26	311.0	43.0	No
95	656,895	5,505,863	104.0	16.1	06/03/18	25.0	0.22	19.9	88.0	No
96	656,635	5,505,857	78.1	7.7	24/05/00	29.0	5.27	371.5	70.0	No
97	659,104	5,505,745	72.0	24.4	01/06/09	24.0	16.42	803.5	48.0	No
98	656,408	5,505,686	110.0	13.4	21/12/99	40.0	1.38	129.6	97.0	No
99	656,220	5,505,662	100.0	8.8	17/11/05	41.4	0.80	72.6	91.0	No
100	661,180	5,505,417	48.0	14.4	18/01/02	3.5	12.10	414.7	33.7	No
101	660,779	5,505,397	157.0	22.0	03/10/13	20.0	0.22	30.2	140.0	No
102	662,146	5,505,380	40.0	5.3	26/08/16	3.6	3.11	103.7	34.7	No
103	661,848	5,505,321	67.5	4.3	23/02/96	35.2	5.96	371.5	63.2	No
104	661,007	5,505,027	51.0	17.3	28/11/96	11.4	8.29	276.5	33.7	No
105	659,748	5,504,944	30.0	17.0	08/02/17	1.5	6.39	83.8	13.0	No
106	661,038	5,504,912	60.0	21.0	19/08/08	4.7	0.57	22.5	40.0	No
107	661,604	5,504,824	82.0	18.5	09/07/11	9.0	0.66	41.5	63.5	No
108	656,754	5,504,398	55.7	31.9	09/10/02	2.3	2.25	53.6	24.0	No
109	658,883	5,504,277	88.0	35.6	03/02/96	30.0	1.64	85.5	52.4	No
110	662,683	5,504,052	49.1	9.5	01/02/97	19.8	241.92	9504.0	39.6	No
111	656,579	5,504,006	54.0	39.4	05/11/10	3.0	3.20	46.7	15.0	No
112	662,987	5,504,001	67.0	7.8	25/04/01	20.0	190.08	11232.0	59.3	No
113	663,739	5,503,952	40.0	2.8	04/05/17	3.5	0.10	3.5	37.2	No
114	658,548	5,503,646	60.0	10.0	02/12/98	1.5	0.07	3.7	50.0	No
115	659,005	5,503,560	60.0	23.8	08/03/99	16.0	2.85	103.7	36.2	No
116	656,104	5,503,544	51.0	41.0	15/11/10	4.5	4.41	44.1	10.0	No
117	660,529	5,503,543	43.7	17.2	29/01/07	7.4	2.33	63.1	26.5	No
118	660,734	5,503,432	48.0	21.6	05/02/09	5.5	2.85	74.3	26.5	No
119	658,394	5,503,135	93.0	29.5	11/02/11	15.0	1.99	129.6	63.5	No
120	661,532	5,502,944	78.0	26.9	29/11/07	25.0	0.60	30.2	51.1	No
121	660,938	5,502,879	96.0	18.0	12/06/14	11.6	0.11	8.6	78.0	No
122	658,655	5,502,812	132.0	34.3	15/03/05	14.0	0.31	30.2	97.7	No
123	655,867	5,502,484	60.0	41.5	07/08/15	3.0	1.30	24.2	19.0	No

Table 6
Average well temperature measured in Osorno in June of 2017.

ID	UTM N m	UTM E m	Temperature °C
O01	5,504,648	661,953	13.35
O02	5,508,105	658,683	13.50
O03	5,503,535	660,521	13.50
O04	5,507,877	653,903	13.37
O05	5,509,744	656,263	14.77
O06	5,505,243	661,070	14.56
O07	5,504,916	661,022	13.72
O08	5,506,498	661,096	13.00
O09	5,505,639	656,356	13.97
O10	5,505,342	656,925	13.58
O11	5,507,475	659,398	12.71

fits well to nature where heat and mass enter a groundwater flow from a point source, which represents the point where groundwater is re-injected into the aquifer after heat pump operation.

The initial and boundary conditions for heat injection at temperature $T > T_0$, where T_0 is temperature of undisturbed groundwater are described as:

$$\lim_{r\to 0}\left(-r\frac{\partial T}{\partial r}\right) = \frac{\dot{Q}\left(T-T_0\right)}{2\pi T} \quad \text{y} \quad T_{r=\infty} = T_0 \tag{8}$$

Here T in the denominator is aquifer transmissivity and $\dot{Q}$ is the water mass flow injected back into the aquifer.

Here the solution for the groundwater temperature at time t, at a distance x and y from the source point, and adjusting according to the retardation coefficient R is the following:

$$\Delta T\left(x,y,t\right) = \frac{\left(T-T_0\right)\dot{Q}}{4\pi\sqrt{\left(\frac{D_L D_T}{R^2}\right)}} e^{\frac{v_x x}{2D_L}} \left[W\left(0,B\right) - W\left(t_D,B\right)\right] \tag{9}$$

Here the integral term is known as the leaky well function or the Hantush–Jacob function which is also written as:

$$\Delta T(x, y, t) = \frac{(T - T_0)\,\dot{Q}}{4\pi\sqrt{\left(\frac{D_L D_T}{R^2}\right)}} e^{\frac{v_x x}{2D_L}} \left[W(0, B) - W\left(t_D, B\right)\right] \tag{10}$$

Here t_D is a dimensionless time expression as follows:

$$t_D = \frac{\left(\frac{v_x}{R}\right)^2 t}{4\frac{D_L}{R}} \tag{11}$$

And B expression is as follows:

$$\sqrt{\frac{v_x^2 x^2}{4D_L^2} + \frac{v_x^2 y^2}{4D_L D_T}} \tag{12}$$

This function is also known as the incomplete Bessel function and is defined as follows:

$$W(u, B) = \int_u^{\infty} \frac{1}{y} e^{-y-\frac{B^2}{4y}}\, dy \tag{13}$$

Srivastava and Guzman-Guzman (1998) indicate the following practical approximations for $W(u, B)$:

$$W(u, B) = W(0, B) - W\left(\frac{B^2}{4u}, 0\right) \quad \text{for} \quad u < u_{min} \tag{14a}$$

$$W(u, B) = W(u, 0) \quad \text{for} \quad u > u_{max} \tag{14b}$$

$$W(u, B) = \frac{1}{2} W(0, B)\,\mathrm{erfc}\left(\alpha X + \beta X^3\right) \quad \text{for} \quad u_{min} < u < u_{max} \tag{14c}$$

Here,

$$X = \ln\left(\frac{2u}{B}\right) \tag{15a}$$

$$\alpha = 0.7708 + 0.3457\ln(B) + 0.09128\,(\ln(B))^2 + 0.09937\,(\ln(B))^3 \tag{15b}$$

$$\beta = 0.02796 + 0.01023\ln(B) \tag{15c}$$

The values of u_{min} and u_{max} are as follows:

$$u_{min} = \max\left(0.06541 B^{0.2763}, 0.02985\right) \quad \text{for} \quad B \le 0.5 \tag{16a}$$

$$u_{min} = 0.1192 B^{1.142} \quad \text{for} \quad B > 0.5 \tag{16b}$$

$$u_{max} = \max\left(39.93 B^{2.391}, 0.02985\right) \tag{16c}$$

The function $W(u, B)$ has several important considerations:

1. $W(u, 0) = W(u)$, and $W(u)$ is known as the exponential integral $E_1(u)$.
2. For large values of u, $W(u, B)$ approaches $W(u, 0)$.
3. $W(0, B) = 2K_0(B)$, where K_0 is the modified Bessel function of the second kind of order 0.

Therefore, we have:

$$W(u, B) = 2K_0 - \mathrm{Ei}\left(\frac{B^2}{4u}\right) \quad \text{para} \quad u < u_{min} \tag{17a}$$

$$W(u, B) = \mathrm{Ei}(u) \quad \text{para} \quad u > u_{max} \tag{17b}$$

$$W(u, B) = K_0\,\mathrm{erfc}\left(\alpha X + \beta X^3\right) \quad \text{para} \quad u_{min} < u < u_{max} \tag{17c}$$

This solution to model the thermal affectation zone describes a situation in nature where heat or mass travel in groundwater from a point source, which represents the injection well. The solution is reduced to a two-dimensional flow with the direction of flow parallel to the x-axis. It is assumed a homogeneous medium with a uniform velocity and that the injection well fully penetrates into the aquifer.

5. Aquifer characterization and input data for calculations

In the case of GWHP, the geometry and hydraulic parameters of the aquifers determine the heat exchange with the ground. In addition, the geometry accounts for the continuity of the permeable medium. On the other hand, the hydraulic parameters along with the hydraulic gradient controls the Darcy velocity of groundwater. Therefore, in this section a detail of this background is indicated for the three cities of interest. The thermal properties of the aquifer and groundwater are also presented, due to their influence on heat transfer calculations. Regarding the operation of the heating system, the aquifer temperature data, the reinjected water flow and its temperature, besides the heating time (months) are indicated. The latter depends on the climatic context of each of the cities.

5.1. Hydrogeological background for each of the cities

The geological context of each city, in addition to hydraulic parameters of shallow aquifers and groundwater temperature are described below.

5.1.1. Talca city

The city of Talca is located on a fluvial fan, where the sedimentary environment is dominated by rivers and channels of low sinuosity and moderate braiding. These channels are characterized by lateral migration (e.g. Knight, 1975). In fact, there are several rivers and channels crossing the city (Fig. 4). In this setting, the flow and sedimentation are confined to rivers and channels, except during floods (Collison, 1996). Therefore, most sedimentary deposits are relatively ephemeral, surviving only a few flood cycles (e.g. Coleman, 1969), and the sedimentary deposits are likely to be truncated by erosion, generating sedimentary units with a limited lateral continuity. Regarding the hydraulic properties, there are significant variations at relatively short distances, accounting for the heterogeneity of the sedimentary infill at the city scale (Fig. 5).

The cross section of Talca (Fig. 5) represents the shallow stratigraphy under the city. The sedimentary infill is mainly composed of gravel (with pebbles and boulders), and sand in variable proportions. There are also fine sand and silt layers to a lesser extent. This record suggests that the sedimentary infill is derived mostly from coarse-grained bedload rivers. These rivers also carry substantial volumes of suspended loads, especially during floods, some of which are deposited in channels and overbank environments (Smith and Smith, 1984). Indeed, in the upper part of the cross section to the east, layers with a higher content of fine sediments are reported. The topographic gradient decreases westward, reducing the energy and capacity for sediment transportation. In addition, there is a rock massif immediately to the west of the city, which constrains the north–south flow of the Claro River (Fig. 4). As a result, the stratigraphy on the western side of the city shows thinner and more alternating layers compared to the eastern side. This feature has been reported in similar settings (Collison, 1996).

The Table 1 summarizes the main hydrogeological data and the calculated hydraulic properties in 26 wells in the city of Talca and its surroundings. Most of the calculated hydraulic conductivity ranges from medium to high, corresponding to values greater than 6 m/day. In 9 wells (36%) the calculated value of hydraulic conductivity is high (< 9 m/day), correlating with a higher proportion of medium to coarse sand. In 10 wells (40%) the calculated value of hydraulic conductivity is medium (6 to 9 m/day), correlating with a higher proportion of fine to medium sand. On the other hand, the hydraulic conductivity is low in 4 wells and very low in just 2 wells, correlating with a higher content of fine sand and silt.

Volcanic sediments are reported in just three well core descriptions, fewer than expected according to the large ash-flows and caldera forming eruptions in the Main Andean Range, 80 km to the east (Hildreth et al., 1984). Volcanic ash layers can generate confined aquifers

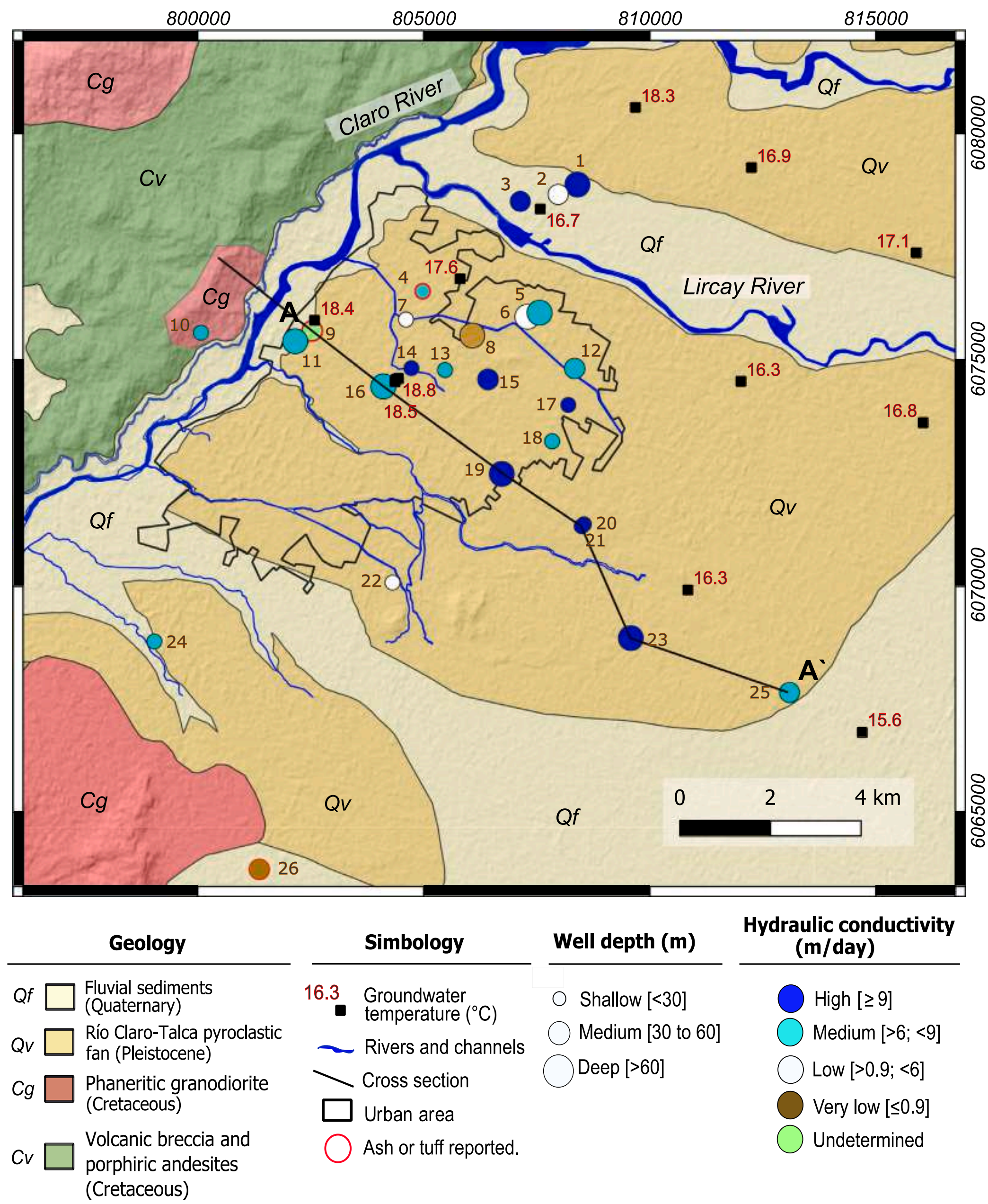

Fig. 4. Well depth, aquifer hydraulic conductivity and average well temperature in Talca. Geology (modified after Varela and Moreno, 1982; Hauser, 1995; Bravo, 2001).

and reduce the hydraulic conductivity of layers containing reworked ash (Custodio and Llamas, 1996) For most wells, the Depth Water Level (DWL) is shallow, with an average depth of 7 m. The maximum value reported is slightly higher than 15 m deep and there are two artesian wells. Since the DWL records are from different dates, the data should be considered as referential.

The Table 2 shows the average temperature from the temperature profiles measured in 34 wells in Talca city and its surroundings. The temperature varies from 15.7 °C to 19.8 °C, with an average value of 17 °C and a standard deviation of 1 °C. The highest temperatures are detected in the central urban area, varying from 18.5 °C to 18.9 °C (Fig. 4).

The calculated hydraulic properties and measured groundwater temperatures in Talca are very favorable for the use of GWHP. Important variations of the hydraulic properties are observed at short distances. Therefore, special care is required to ensure that groundwater is extracted and reinjected into the same aquifer to maintain hydraulic balance and avoid mixing of aquifers. Despite this caution, the potential is very good. In fact, the Talca regional hospital uses GWHP to provide heating and cooling. The well number 16 (Fig. 4) corresponds to one of the wells of this geothermal system.

5.1.2. Temuco city

Most of the urban area of Temuco city is located along the Cautín river (Fig. 6). This river has a low sinuosity and moderate braiding. In this sedimentary environment, the flow and sedimentation are confined to the river, except during floods (Collison, 1996). The geological setting is similar to that of Talca but concentrated in one river. The fluctuation in river discharge results in alternating layers of matrix-filled and open-worked gravel within the river bars (Smith, 1974). Currently, sediments accumulate on the river floor to split the flow at several coexisting scales, and the erosion of the flank bars generates successive events of erosion and deposition. Furthermore, slug channels become active during higher stages of flooding and accumulate fine-grained sediments during lower stages (Bluck, 1974). In this setting, most sedimentary deposits are relatively ephemeral surviving only a

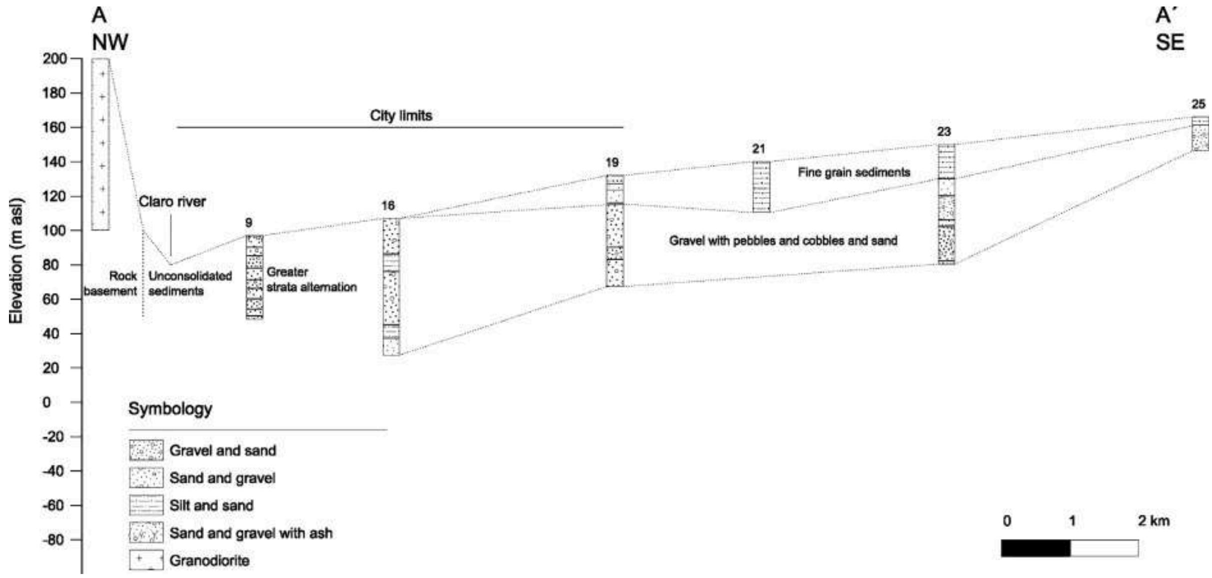

Fig. 5. NW to SE cross section of Talca city based on the stratigraphy of wells 9, 16, 19, 21, 23, and 25.

few flood cycles or bar migration (e.g. Coleman, 1969). Therefore, the deposits are likely to be truncated by erosion, generating sedimentary units with a limited lateral continuity. Regarding the hydraulic properties within the Cautín River belt, which is the area where the river has deposited and eroded, there are significant variations at relatively short distances. The above accounts for the heterogeneity of the sedimentary infill at the city scale. Outside the river belt, there are sedimentary deposits from alluvial, glacial, and volcanic origin (Fig. 7).

The cross section of Temuco (Fig. 7) represents the shallow stratigraphy under the city. Within the Cautín river belt domain, most sediments range from gravel with pebbles to fine sand. As the flow over a bar is reduced, silt and sand that is carried in saltation or suspension is deposited in static gravel, filling the pore space, or accumulating on top. Therefore, silt and clay size sediments are reported in well records within the river belt domain. Moving away perpendicularly from the mainstream river, northward and southward, in the upper part of the cross section dominates silt and clay-sized sediments, which could have been deposited during flood events. To the north of the river, the wells reach glacial origin sediments, which have an important effect on the hydraulic properties of the medium due to the fine particles content. Furthermore, both north and south of the river, bedrock is reported at depths in the range of 40 to 60 m deep.

The Table 3 summarizes the main hydrogeological data and the calculated hydraulic properties in 47 wells in the city of Temuco and its surroundings. Most of the calculated hydraulic conductivity ranges from low to very low (> 6 m/day). In 17 wells (36%) the calculated hydraulic conductivity is low (6 to 0.9 m/day), correlating with a higher proportion of fine sand. In 20 wells (43%) the calculated hydraulic conductivity is very low (> 0.9 m/day), correlating with a higher proportion of fine sand, silt and clay. On the other hand, the hydraulic conductivity is medium in 3 wells and high in 7 wells, correlating with a higher content of medium to coarse sand.

Volcanic sediments are reported in just four well core records, fewer than expected if we consider the presence of at least three active stratovolcanoes in the Main Andean Range, 70 km to the east. As mentioned above, volcanic ash layers can generate confined aquifers and reduce the hydraulic conductivity of layers containing reworked ash due to their impermeable behavior (Custodio and Llamas, 1996). For most wells, the Depth Water Level (DWL) is shallow with an average value of 13 m depth. The maximum DWL is slightly deeper than 37 m. Because the DWL records are from different dates, they should be considered as referential.

The Table 4 shows the average temperature obtained from the temperature profiles measured in 11 wells in Temuco city and its surroundings. The temperature ranges from 12.8 °C to 14.8 °C, with an average value of 14.0 °C and a standard deviation of 0.6 °C. The lowest temperature was measured in the well closest to the Cautín River (Fig. 6), which suggests that the thermal influence of the Cautín River could reach tens of meters into the aquifer.

The calculated hydraulic properties and measured groundwater temperatures in the Cautín river belt domain are very favorable for the use of GWHP. The variations of the hydraulic properties are observed at short distances, consistent with the limited lateral extension of the sedimentary deposits. Therefore, special care is required to ensure that groundwater is extracted and reinjected into the same aquifer to maintain hydraulic balance and avoid aquifer mixing. Outside of the river belt domain, hydraulic conductivity is low to very low, so GWHP might not be a feasible alternative.

5.1.3. Osorno city

The city of Osorno is located at the confluence of the Rahue and Damas rivers (Fig. 8). Therefore, much of the city is located on the sediments of both river belts. Nevertheless, there are significant areas of the city on sediments of volcanic and glacial origin. Both the Rahue river and the Damas river are low sinuosity and moderately braided. As in Talca and Temuco, fluvial sedimentation is confined to the rivers except during floods (Collison, 1996) and most sedimentary deposits are relatively ephemeral, surviving only a few flood cycles (Coleman, 1969). The migration of permanent or intermittent stream flows is also characteristic of this sedimentary environment (e.g. Knight, 1975). Therefore, the sedimentary deposits of each sedimentary event are likely to be truncated by erosion, and consequently there is a limited lateral continuity of the sedimentary layers. On the other hand, in glacial environments intensive shearing and abrasion occurs, so sediments may be layered but not sorted and rock flour is abundant. Glacial sedimentary processes commonly overlap with processes in other environments, for example fluvial reworking (Miller, 1996). Regarding the hydraulic properties, within the Damas River belt there are significant variations at relatively short distances, accounting for the heterogeneity of the sedimentary infill at the city scale. Outside the river belt, there are sedimentary deposits of glacial and volcanic origin, where the calculated hydraulic conductivities are low to very low (Fig. 8).

The cross section of Osorno (Fig. 9) represents the shallow stratigraphy under the city. In the central-eastern sector of the city, the

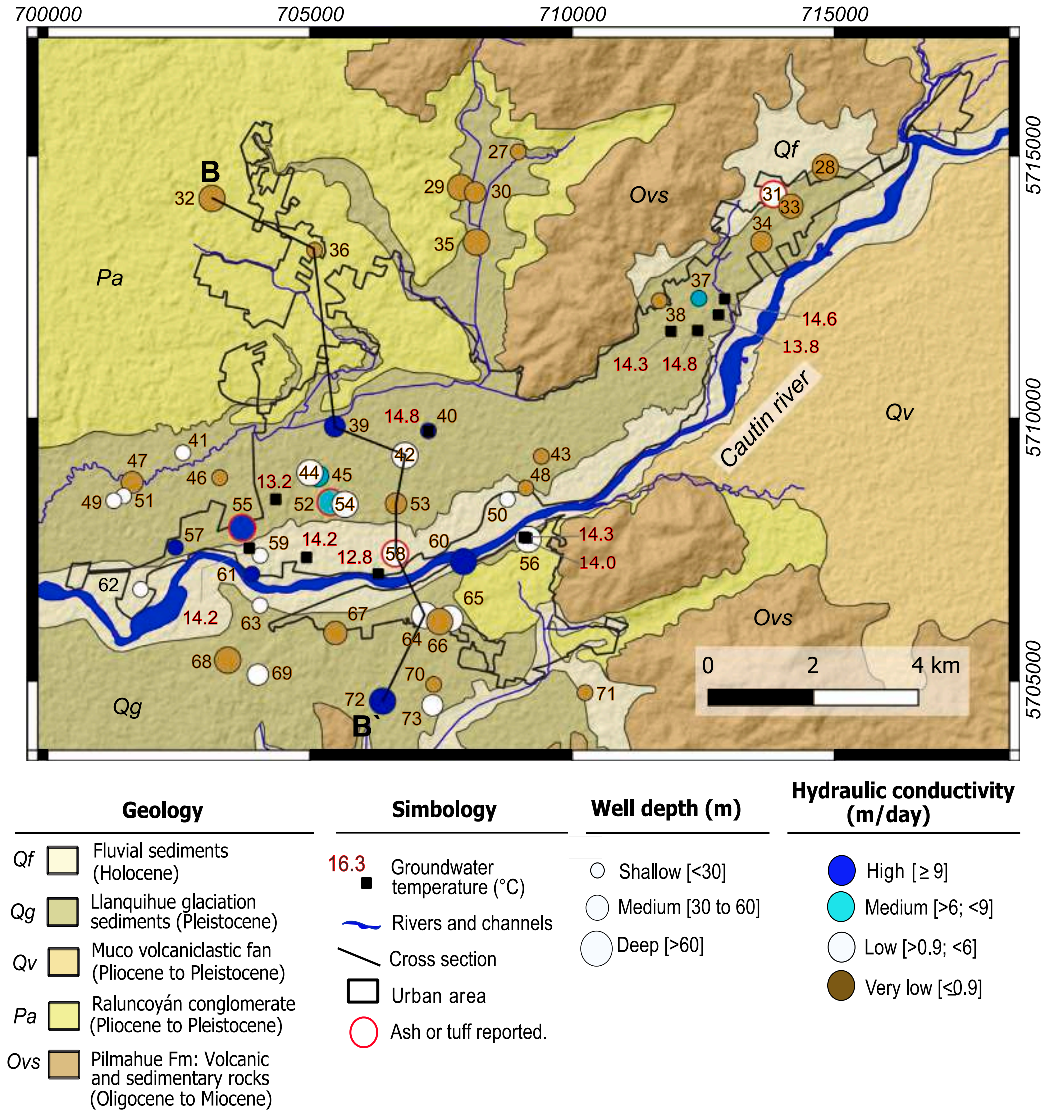

Fig. 6. Well depth, aquifer hydraulic conductivity and average well temperature in Temuco. Geology (modified after Mella and Quiroz, 2010).

sediments up to 50 m depth were deposited in a fluvial and glaciofluvial environments associated with the Rahue and Damas rivers, respectively. These sediments range from pebble-gravel to fine sand. In addition, silt and clay layers are reported in many well descriptions. In the upper part of the cross section, in between the Damas and Rahue rivers, sand and clay-sized sediments dominate, which might have been deposited during flood events (Fig. 9). In the central-western sector, in the area that surrounds the Rahue river, diverse types of glacial sediments are recorded. Stands out, a thick layer of clay and sand, which may have a glaciolacustrine or distal fluvioglacial origin. At the base of these finer sediments there are till deposits from subglacial or periglacial environments (Miller, 1996). There are also interbedded fine-grained sediments within the till deposits. These deposits extend from west to east under the fluvial and glaciofluvial deposits that underlie the city (Fig. 9).

The Table 5 summarizes the main hydrogeological data and the calculated hydraulic properties in 50 wells in the city of Osorno and its surroundings. In most wells the calculated hydraulic conductivity is low to very low (< 6 m/day). In 22 wells (44%) the hydraulic conductivity is low (6 to 0.9 m/day), correlating with a higher proportion of fine sand. In 17 wells (34%) hydraulic conductivity is very low (< 0.9 m/day), correlating with a higher proportion of fine sand, silt, and clay. On the other hand, the hydraulic conductivity is medium in 3 wells and high in 8 wells, correlating with a higher proportion of medium to coarse sand and even clean gravel.

Volcanic sediments are reported in just one well, fewer than expected since Quaternary ignimbrites with a thickness of ~1 m were reported near the city of Osorno (Lara et al., 2006). As in Talca and Temuco, volcanic ash layers can generate confined aquifers and reduce the hydraulic conductivity of layers containing reworked ash (Custodio and Llamas, 1996). For most wells, the Depth Water Level (DWL) was moderately deep, with an average depth of 21 m; deeper than Talca (Table 1) and Temuco (Table 3). In 13 wells the DWL was deeper than 29 m, all of them located in high areas along the north, west and south of the city, 30 to 50 m above the Rahue River level. The two deepest wells, located on the western edge of the city (86 and 81 in Fig. 8), had a DWL of 58 m and 60 m (Table 5). Because the DWL records are from different dates, the data should be considered as referential.

The Table 6 shows the average temperature obtained from the temperature profiles measured in 11 wells in Osorno city and its surroundings. The temperatures vary from 12.7 °C to 14.8 °C, with an average value of 13.6 °C and a standard deviation of 0.6 °C (Table 6). The distribution of groundwater temperatures is very homogeneous within the city limits.

The calculated hydraulic properties and measured groundwater temperatures at Osorno are very favorable for the use of GWHP within

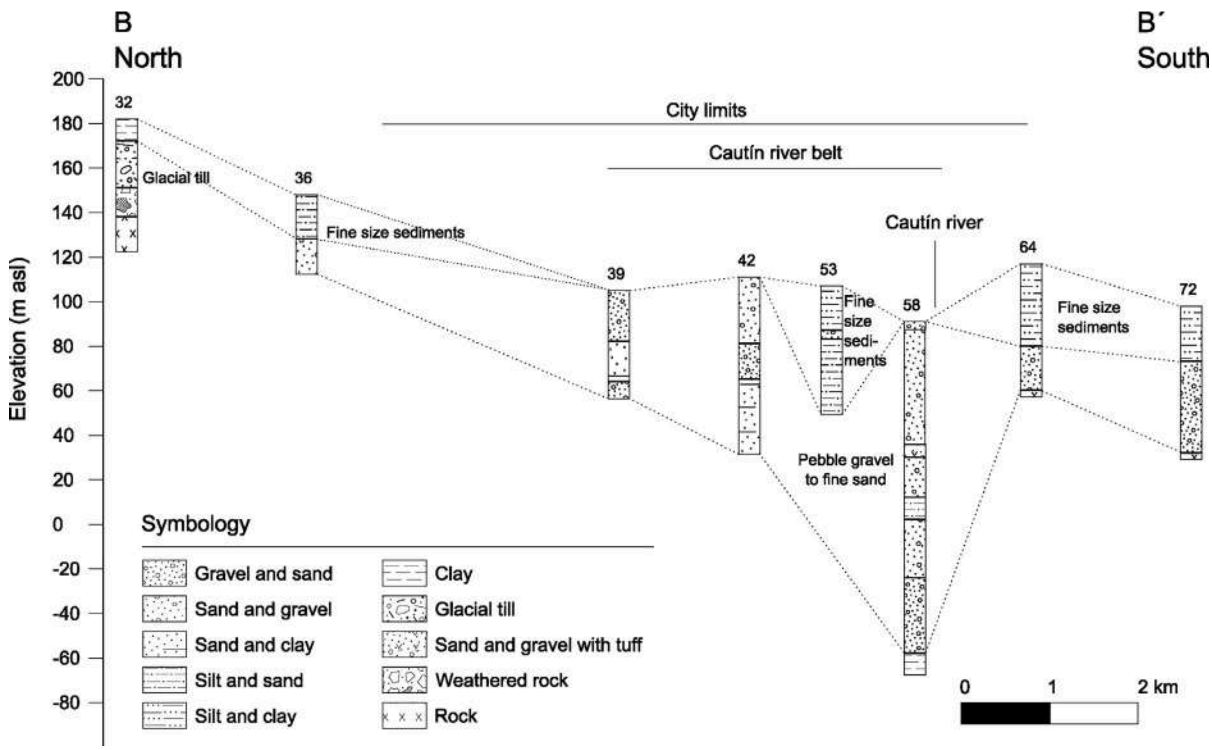

Fig. 7. N–S cross section of Temuco city based on the stratigraphy of wells 32, 36, 39, 42, 53, 58, 64, and 72.

Table 7
Values of initial conditions for the analytical calculation of heat and mass transport from a reinjection well.

	Talca			Temuco			Osorno		
Aquifer thickness [m]	37	37	3	40	40	40	54	54	54
Hydraulic conductivity [m/s]	3.90E−05	8.10E−05	1.70E−04	6.15E−06	1.50E−05	4.65E−05	6.95E−06	2.15E−05	5.85E−05
hydraulic gradient	0.0062	0.0062	0.0062	0.004	0.004	0.004	0.004	0.004	0.004
Darcy velocity of groundwater [m/yr]	7.63	15.84	33.24	0.78	1.89	5.87	0.88	2.71	7.38
Porosity	0.21	0.26	0.26	0.21	0.21	0.21	0.21	0.21	0.21
Aquifer thermal conductivity [W/m°C]	1.56	1.86	1.86	1.56	1.56	1.56	1.56	1.56	1.563
Aquifer volumetric heat capacity [MJ/m^3°C]	2.165	1.9	1.9	2.165	2.165	2.165	2.165	2.165	2.165
Water volumetric heat capacity [MJ/m^3°C]	4.19	4.19	4.19	4.19	4.19	4.19	4.19	4.19	4.19
Extraction/reinjection rate [m^3/s]	0.005	0.005	0.005	0.005	0.005	0.005	0.005	0.005	0.005
Undisturbed aquifer temperature [°C]	17	17	17	14.1	14.1	14.1	13.4	13.4	13.4
Reinjection temperature (ΔT = 3 °C) [°C]	14	14	14	11.1	11.1	11.1	10.4	10.4	10.4
Heating time [months]	6	6	6	7	7	7	9	9	9

the Damas river belt domain. The fluvial to glaciofluvial sediments corresponding to this river belt have a limited lateral extension. Within this domain, the variations of the hydraulic properties at short distances are observed. Therefore, as in Talca and Temuco, special care is required to ensure that the groundwater is extracted and reinjected into the same aquifer to maintain hydraulic balance and avoid mixing of aquifers. Outside of the Damas river belt domain, hydraulic conductivity is mainly low to very low, so GWHP might not be a viable alternative.

5.2. *Synthesis of input data for calculations*

The input data for the calculation of the thermal zone affected by the GWHP operation in the three cities of interest are shown in Table 7. These values are used as initial conditions for the analytical calculation of heat and mass transport from the reinjection well. The analysis to obtain these values is presented in the following subsections.

5.2.1. *Aquifer thickness*

The thickness of the aquifer [m] in each of the three cities was determined as the average value of the saturated thickness. The above, according to the wells considered for the hydraulic characterization (Tables 1, 3, and 7).

5.2.2. *Aquifer hydraulic parameters and Darcy velocity of groundwater*

The hydraulic conductivity values [m/s] were calculated from the pumping tests. Since these values in Talca, Temuco and Osorno fit to a normal distribution, it is possible to treat the data based on their statistical distribution. Considering that the hydraulic conductivity values cover several orders of magnitude, a logarithmic scale is used on the *x*-axis for better visualization (Fig. 10). To analyze the effects of variations in hydraulic conductivity, three values were considered in each of the cities: percentile 25 (q1), percentile 50 (q2), and percentile 75 (q3).

In Talca, the calculated hydraulic conductivities are higher than in Temuco and Osorno, probably due to the predominance of gravel (with boulders and pebbles) and sand in varying proportions deposited in a fluvial fan environment. In contrast, in the cities of Temuco and Osorno, the coarse-grained deposits are restricted to the river belts, but outside these environments there are sediments of glacial, alluvial, or volcanic origin, which are characterized by a higher content of fine sediments that reduce hydraulic conductivity (Custodio and Llamas, 1996). The hydraulic conductivity distributions in Temuco and Osorno cities are similar, being slightly higher in Osorno, accounting for a similar depositional environment in both cities. In Temuco and Osorno, there are more outlier values, reaching high to very high hydraulic

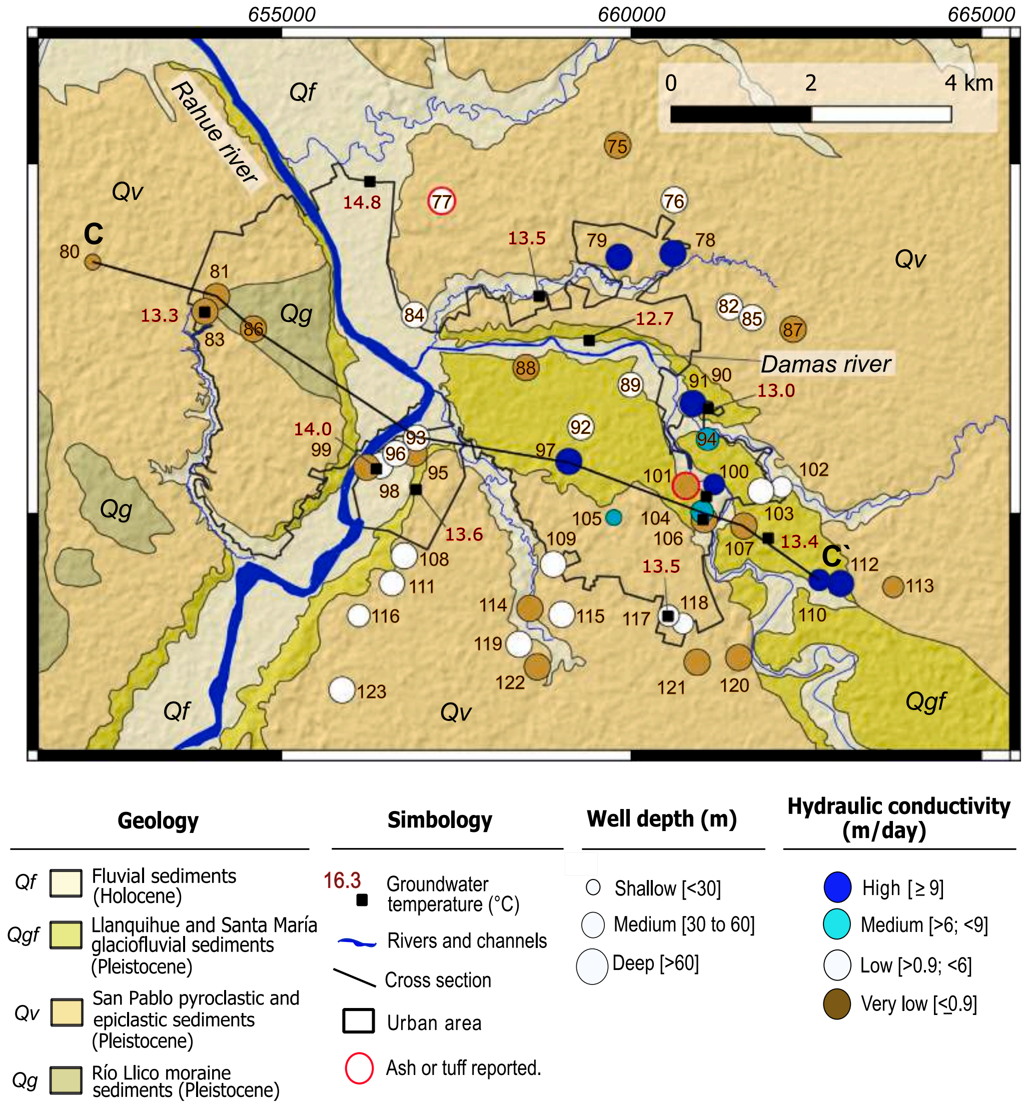

Fig. 8. Well depth, aquifer hydraulic conductivity and average well temperature in Osorno. Geology (modified after Pérez et al., 2003).

conductivities (Fig. 10). The latter since in fluvial and glaciofluvial environments there are deposits of coarse sand or gravel, with high to very high hydraulic conductivity. These deposits are opposed to the more frequent ones, which contain varying proportions of sand, silt, and clay.

Considering the results of hydraulic conductivities for p50 and p75, sand and gravel predominate in the city of Talca, which corresponds to a porosity value of 0.26 (Custodio and Llamas, 1996), for p25, which is related to fine sand, corresponds a porosity value of 0.21 (Custodio and Llamas, 1996). Likewise, in the cities of Temuco and Osorno fine sand predominates, which corresponds to a porosity value of 0.21.

The Darcy groundwater velocity [m/yr] is calculated by multiplying the hydraulic gradient and the hydraulic conductivity. For this work, a representative value of hydraulic gradient was used for each city (DGA, 2012, 2013). From these hydraulic gradients, three Darcy velocity values were obtained for each city, since three hydraulic gradients q1, q2 and q3 are considered.

5.2.3. Thermal properties of the aquifer and groundwater

From the stratigraphic record in wells and the calculated hydraulic conductivity values, the main types of sediments can be established. From these sediments it is possible to establish the values of the thermal properties from the literature (Dalla Santa et al., 2020). For the calculations, the thermal conductivity [W/m°C] and the volumetric heat capacity [MJ/m^3°C] of the aquifer are required. On the other hand, these values of thermal properties in water are well known. The undisturbed temperature of the aquifer [°C] is obtained as the average of the values measured in each city (Tables 2, 4 and 6).

5.2.4. Extraction/reinjection rate and aquifer temperature related to system operation

The average rate of groundwater extraction in the wells of the cities of interest is at least 5.5 [L/s], in the city of Temuco (see Tables 1, 3, and 5). Therefore, an extraction/reinjection rate of 5 [L/s] is considered here. In addition, a recovery of 3 [°C] is considered to evaporate the refrigerant in the heat pump. This value considers the optimization of the use of groundwater and thermal effects on the aquifer (Arola et al., 2014).

The heating time considered in the analytical calculations is different for each city and depends on the average monthly temperatures. A temperature below 14 °C was considered to establish the need for heating. For its estimation, the agroclimatic atlas of Chile was used (Santibáñez Quezada, 2017a,b,c).

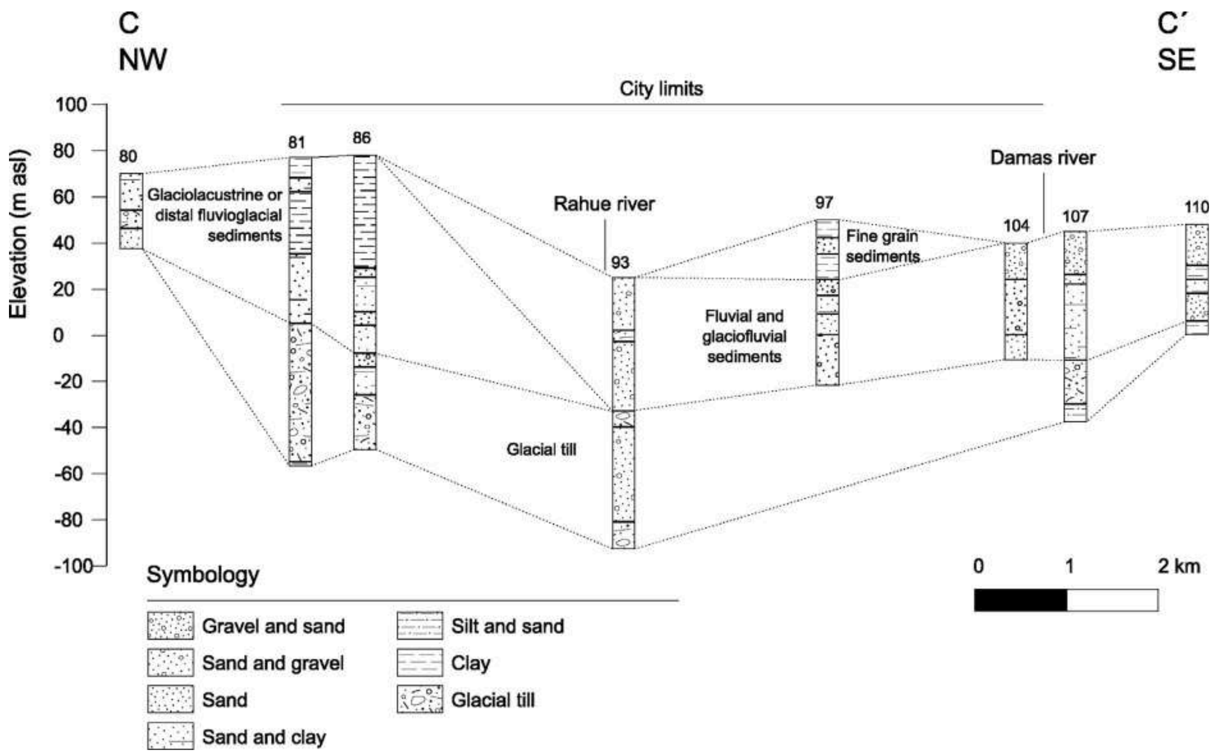

Fig. 9. NW-SE cross section of Osorno city based on the stratigraphy of wells 80, 81, 86, 93, 97, 104, 107, and 110.

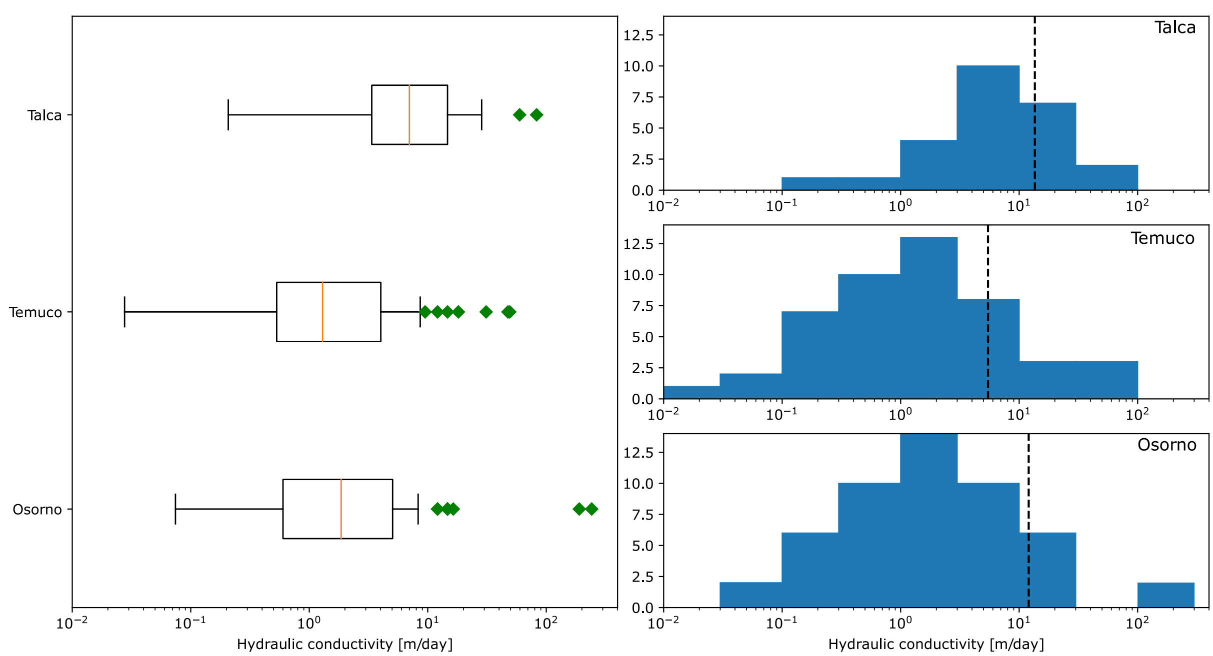

Fig. 10. Hydraulic conductivity distribution for each studied city obtained from the analyzed pumping test. On the left, boxplots are shown. The box extends from the first quartile to the third, with a line at the median. The whiskers extend from the box 1.5 times the interquartile range.

6. Results

The calculations of the TAZ are shown in Fig. 11, which corresponds to the plane where the thermal affectation has the greatest spatial reach. For each of the cities, three results are shown that correspond to the percentiles of the hydraulic conductivity values p25, p50 and p75 (Fig. 10). These hydraulic conductivities have a directly proportional effect on the Darcy velocity. Therefore, they have an effect on the shape of the TAZ elongation in the groundwater flow direction.

The largest extension of the TAZ in the direction of the groundwater flow is in the city of Talca, where it reaches approximately 30 m from the reinjection well. The above, considering the heating time of 6 [months] in that city, which is lower compared to Temuco and Osorno.

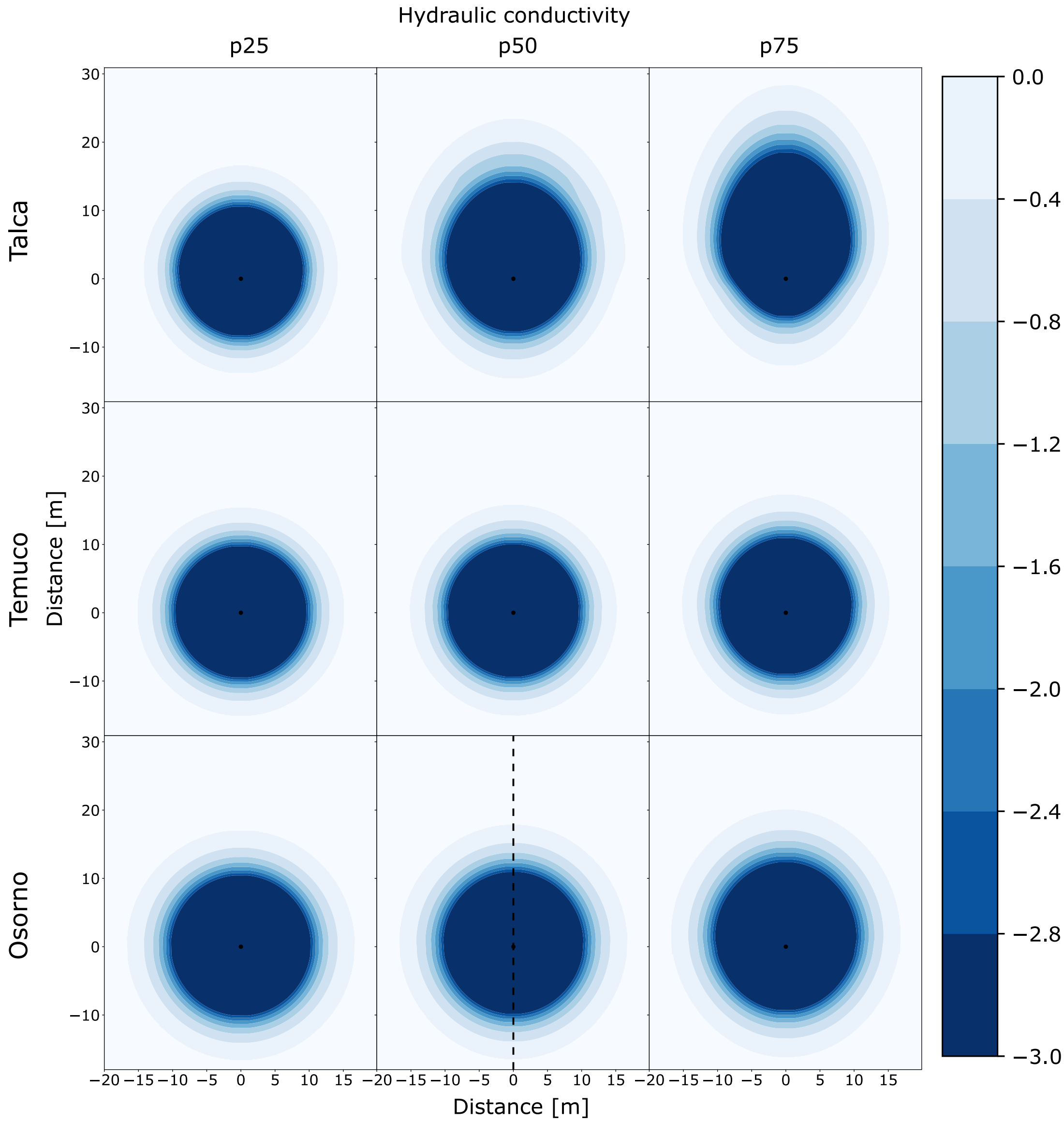

Fig. 11. Injection area zoom views. The area corresponds to the plane where the thermal affectation has the greatest spatial reach. The direction of groundwater flow in the figure is shown upwards. Dashed line corresponds to the profile location of Fig. 12 for 5 L/s.

Although heating time is lower in Talca, the TAZ presents a greater dispersion due to the greater Darcy velocity of groundwater flow.

In the cities of Temuco and Osorno, the TAZ is less elongated than in the city of Talca due to the lower Darcy velocity, which is related to lower hydraulic conductivity. Nevertheless, in the case of the p75 of hydraulic conductivity, it can be seen that the groundwater flow is greater in Osorno than in Temuco, which generates a more elongated TAZ. Because of the lower temperature dispersion due to the effect of groundwater flow, the TAZ in the cities of Temuco and Osorno is more concentrated around the reinjection well. The above generates that the TAZ has a greater reach in the opposite direction to the groundwater flow, which would be the commonly chosen location of the pumping well. The effect of the longer heating time in Osorno than in Temuco is better observed for the case of the P25 of hydraulic conductivity, where the TAZ has a greater reach in the case of Osorno.

Considering that in the city of Osorno the TAZ has the greatest reach in the opposite direction of the groundwater flow, calculations of the TAZ were carried out for three reinjection rates: 3, 5, and 10 [L/s]. For the three calculations, the p50 of hydraulic conductivity is considered. The Fig. 12 shows the greatest extent of the TAZ in a graph of temperature difference generated by reinjection and distance from reinjection well. The graph corresponds to a temperature profile that is parallel to the groundwater flow and that crosses the reinjection well (see Fig. 11 for profile location). From these calculations it can be seen that the extent of the TAZ varies slightly as the reinjection rate varies. For the three reinjection rates, the area of greatest thermal affectation reaches approximately 10 m. The temperature difference between the reinjected water and the undisturbed aquifer is sharply reduced from 10 to 20 m from the reinjection well.

For all the cases and cities, it can be seen that the TAZ has a moderate to slight modification due to the effect of the groundwater flow, being concentrated and close to the reinjection well. Notwithstanding, a greater elongation and temperature dispersion is observed for the case of the highest hydraulic conductivities. The above is clear in the city of Talca.

According to the results, for a reinjection rate of 5 [L/s] and a heat recovery of 3 [°C], the greatest extent of the TAZ in the direction of

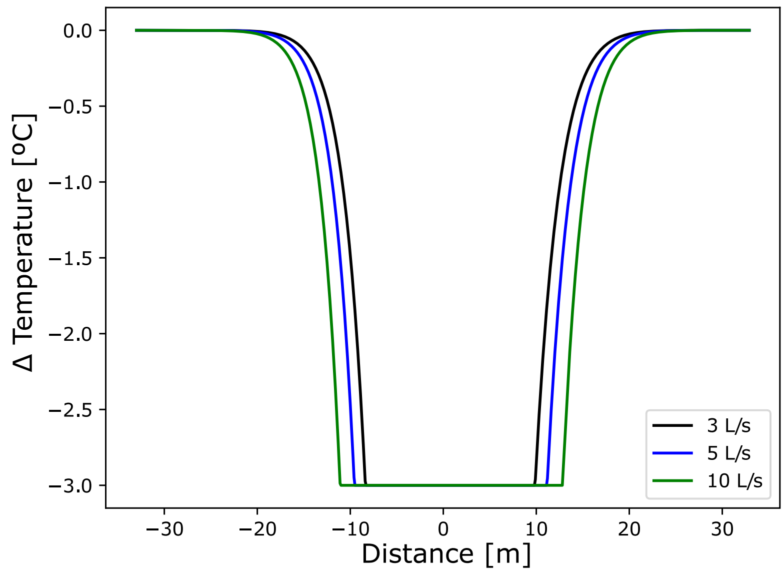

Fig. 12. Relationship between the temperature of the affected thermal zone in a line parallel to groundwater flow in Osorno city for 3, 5 and 10 [L/s] reinjection rates (see Fig. 11 for location of profile).

the groundwater flow is reached in the city of Talca, which reaches approximately 30 m. Osorno is the city in which the greatest extension of the TAZ is reached in the opposite direction to the groundwater flow, where for reinjection rates of 3, 5 and 10 [L/s], the TAZ reaches up to approximately 20 m.

The calculated TAZ is in the order of tens of meters are comparable with calculations for specific projects of a comparable magnitude to the cases calculated in this work (e.g., Lo Russo et al., 2012).

7. Discussion

The following discussions are related to the performance of GWHP systems for heating and cooling, and the available thermal power of the calculated cases.

7.1. Temperature distribution and GWHP efficiency

The efficiency of GWHP is controlled by the aquifer temperature and functioning temperature of the heating distribution system. The Fig. 13 shows the distribution of groundwater temperature measured in the three cities (Tables 2, 4, and 6). In Talca, the groundwater temperature is approximately 3 °C higher than in Temuco and Osorno, which is consistent with higher mean annual atmospheric temperatures. The higher groundwater temperatures observed in Talca could result in better heating performances but would result in efficiency decrease for cooling purposes compared with Temuco and Osorno. The higher temperature measured in Talca downtown could be caused by a Subsurface Urban Heat Island (SUHI) effect that must be considered for GWHP design (Huang et al., 2009; Zhu et al., 2010; Perego et al., 2021).

The GWHP efficiency corresponds to the relation between the energy used for climatization versus the energy consumed by the system. The Coefficient of Performance (COP) is calculated for heating efficiency and the Energy Efficiency Ratio (EER) for cooling efficiency. An approximation of the efficiency can be obtained from the Carnot cycle and an efficiency factor, which corresponds to 0.5 for heating and cooling (Morrone et al., 2014). With the above, the efficiency in the case of heating and cooling is calculated as follows:

$$COP = 0.5\frac{T_{hot} + 273}{T_{hot} - T_{cold}} \tag{18a}$$

$$EER = 0.5\frac{T_{cold} + 273}{T_{hot} - T_{cold}} \tag{18b}$$

The average groundwater temperature [°C] is considered as the cold temperature (T_{cold}) for heating purpose, is considered as hot temperature (T_{hot}) for cooling purposes. Conversely, the temperature of the distribution system is considered as hot (T_{hot}) for heating purposes, and cold (T_{cold}) for cooling purposes. This nomenclature considers the heat pump point of view that moves heat from a cold source to a hot source by the mechanical work of the compressor. Heating and cooling distribution systems are diverse and, depending on the system, require different operating temperatures. Here, three types of distribution systems are considered: radiators, fan coils and radiant floor. For heating purposes, (T_{hot}) of the distribution system is 60 °C (radiator), 50 °C (fan coil), and 40 °C (radiant floor). On the other hand, for cooling purposes (T_{cold}) of the distribution system is 7 °C (fan coil), and 15 °C (radiant floor). It is not considered radiators for cooling, because of the condensation issues on the surface of cooling devices.

Efficiency results for the three cities and for each heat distribution system are compared in Fig. 14, except for cooling with the radiant floor, since (T_{hot}) and (T_{cold}) are very similar (even reversed). The use of radiators for heating with GWHP is not recommended due to the low efficiency (in Fig. 14, COP < 4). The highest efficiencies are reached with radiant floor for heating and cooling. The energy consumption in the pumping well was not considered for the efficiency calculation, which reduces the global efficiency of GWHP.

7.2. Available power for the use of GWHP

The power available for heating that comes from the aquifer ($P_{aquifer}$) can be calculated as follows:

$$P_{aquifer} = \dot{Q}\rho_w c_w \Delta T \tag{19}$$

Here, $\dot{Q}$ is the flow rate [m^3/s], ρ_w is the water density [kg/m^3], c_w is the water specific heat capacity [J/(kg°C)], and ΔT is the temperature difference between extracted and reinjected groundwater [°C].

Therefore, for the flow rate of 5 [L/s], and a temperature difference of 3 [°C], the thermal power coming from the aquifer is about 60 kW. The thermal power from the operation of these systems (P_{tot}) is slightly higher because the total power for heating purposes is calculated as follows:

$$P_{tot} = \frac{COP}{(COP - 1)P_{aquifer}} \tag{20}$$

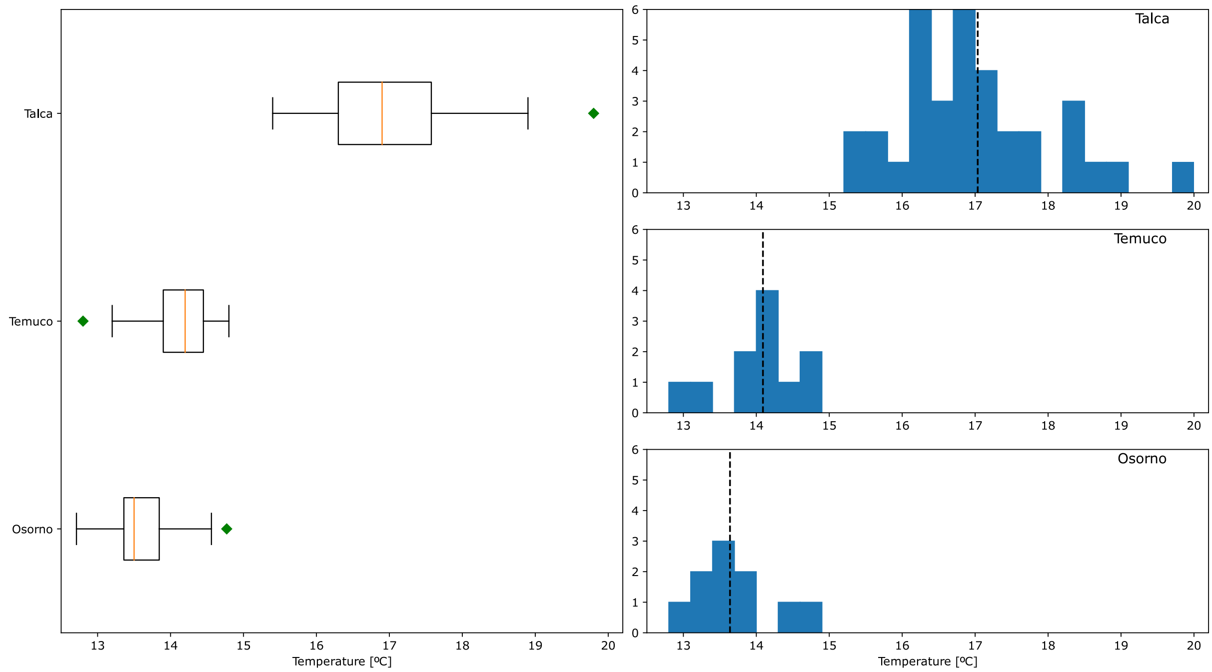

Fig. 13. Distribution of aquifer temperature for each city. On the left, boxplots are shown. The box extends from the first quartile to the third, with a line at the median. The whiskers extend from the box 1.5 times the interquartile range. Outliers are those past the end of the whiskers. On the right, histograms for each city are shown and the dashed line corresponds to the mean.

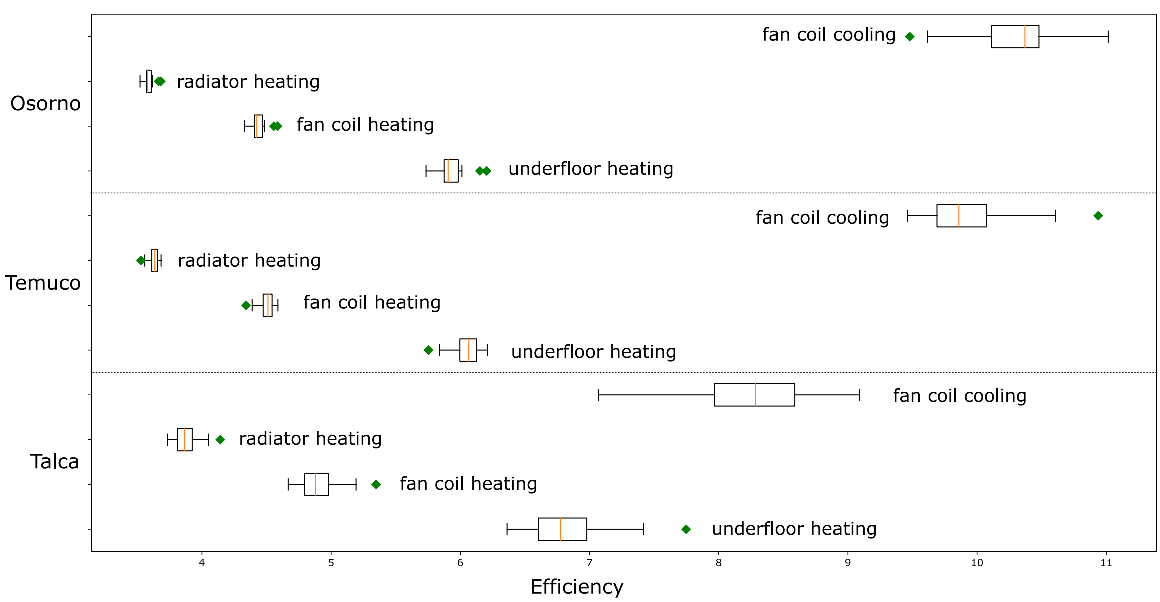

Fig. 14. Efficiency distribution illustrated in a boxplot for each studied city and for each distribution system. The box extends from the first quartile to the third, with a line at the median. The whiskers extend from the box 1.5 times the interquartile range. Outliers are those past the end of the whiskers.

Despite the work required in pumping water, this order of magnitude of power is consistent with geothermal heat pump heating projects registered in the south-central zone of Chile, including schools and small-scale district heating systems for tens of houses. These systems provide heating to spaces in the order of one thousand square meters (Morata et al., 2020).

8. Conclusion

In Talca city the aquifer is mainly composed of gravel, and sand in variable proportions, which correlates with medium to high hydraulic conductivity. Therefore, hydraulic conditions are very favorable for the use of GWHP. In Temuco and Osorno cities, just within the domains of the river belts the aquifers are composed of sand and gravel, yet outside of these domains fine-grained sediments predominate. Consequently, in both cities, most of the calculated hydraulic conductivities are low to very low, with the exception of the aquifers located in the specific river belts, where the calculated hydraulic conductivities are medium to high. Therefore, close to rivers the hydraulic conditions are favorable for the use of GWHP, but outside of the river belt domains GWHP might not be a viable alternative.

The groundwater temperature is very favorable for heating and cooling with GWHP in the three cities of interest. In particular, in downtown Talca there is a positive thermal anomaly, which enhances the performance for heating purposes.

For all the cases and cities, the calculated TAZ has a moderate to slight elongation due to the effect of the groundwater flow, being well concentrated and close to the reinjection well.

The highest TAZ elongation and temperature dispersion in the aquifer is reached in the city of Talca, which coincides with a higher calculated hydraulic conductivity. On the other hand, the greatest TAZ and the greatest reach in the opposite direction to the flow of groundwater are calculated in the city of Osorno. This is due to the longer time of use for heating and the hydraulic properties, which are not as low as in Temuco, but are also classified in a range from low to very low hydraulic conductivity.

CRediT authorship contribution statement

Mauricio Muñoz: Writing – review & editing, Writing – original draft, Project administration, Methodology, Investigation, Formal analysis, Conceptualization. **Diego Aravena:** Writing – review & editing, Writing – original draft, Methodology, Investigation, Formal analysis, Conceptualization. **Karin García:** Writing – review & editing, Writing – original draft, Software, Methodology, Investigation, Formal analysis, Conceptualization. **Nicolás Hurtado:** Writing – original draft, Methodology, Investigation, Formal analysis. **Esteban Micco:** Writing – original draft, Investigation, Formal analysis. **Diego Morata:** Writing – review & editing, Writing – original draft, Investigation, Funding acquisition, Formal analysis, Conceptualization.

Declaration of competing interest

The authors declare that they have no known competing financial interests or personal relationships that could have appeared to influence the work reported in this paper.

Data availability

Data will be made available on request.

Acknowledgments

This work has been supported by the ANID-FONDAP Project number 15200001 and ACE210005 (Centro de Excelencia en Geotermia de los Andes, CEGA, Chile). The authors would especially like to thank the students who participated in the field-work in Talca, Temuco, and Osorno.

Appendix A. Supplementary data

Supplementary material related to this article can be found online at https://doi.org/10.1016/j.jsames.2022.104135.

References

Arola, T., Eskola, L., Hellen, J., Korkka-Niemi, K., 2014. Mapping the low enthalpy geothermal potential of shallow quaternary aquifers in Finland. Geotherm. Energy 2, 9. http://dx.doi.org/10.1186/s40517-014-0009-x.

Banks, D., 2009. Thermogeological assessment of open-loop well-doublet schemes: A review and synthesis of analytical approaches. Hydrogeol. J. 17, 1149–1155. http://dx.doi.org/10.1007/s10040-008-0427-6.

Banks, D., 2011. The application of analytical solutions to the thermal plume from a well doublet ground source heating or cooling scheme. Q. J. Eng. Geol. Hydrogeol. 44 (2), 191–197. http://dx.doi.org/10.1144/1470-9236/09-028, URL https://www.lyellcollection.org/doi/abs/10.1144/1470-9236/09-028, arXiv: https://www.lyellcollection.org/doi/pdf/10.1144/1470-9236/09-028.

Banks, D., 2012. An Introduction to Thermogeology: Ground Source Heating and Cooling. John Wiley & Sons.

Bear, J., 1972. Dynamics of Fluids in Porous Media. American Elsevier Publishing Company, New York, p. 764.

Beardsmore, G.R., Cull, J.P., 2001. Thermal gradient. In: Crustal Heat Flow: A Guide to Measurement and Modelling. Cambridge University Press, pp. 47–89. http://dx.doi.org/10.1017/CBO9780511606021.004.

Bluck, B.J., 1974. Structure and directional properties of some valley Sandur deposits in southern Iceland. Sedimentology 21 (4), 533–554. http://dx.doi.org/10.1111/j.1365-3091.1974.tb01789.x, URL https://onlinelibrary.wiley.com/doi/abs/10.1111/j.1365-3091.1974.tb01789.x, arXiv: https://onlinelibrary.wiley.com/doi/pdf/10.1111/j.1365-3091.1974.tb01789.x.

Bravo, P., 2001. Geología del Borde Oriental de la Cordillera de la Costa entre los Ríos Mataquito y Maule, VII Región (B.s. thesis). Universidad de Chile.

Chiasson, A.D., 2016. Geothermal Heat Pump and Heat Engine Systems: Theory and Practice. John Wiley & Sons, Ltd, http://dx.doi.org/10.1002/9781118961957.ch3, URL https://onlinelibrary.wiley.com/doi/abs/10.1002/9781118961957.ch3, arXiv: https://onlinelibrary.wiley.com/doi/pdf/10.1002/9781118961957.ch3.

Clauser, C., 1997. Geothermal energy use in Germany— status and potential. Geothermics 26 (2), 203–220. http://dx.doi.org/10.1016/S0375-6505(96)00040-5, URL https://www.sciencedirect.com/science/article/pii/S0375650596000405.

Coleman, J.M., 1969. Brahmaputra river: Channel processes and sedimentation. Sediment. Geol. 3 (2), 129–239. http://dx.doi.org/10.1016/0037-0738(69)90010-4, URL https://www.sciencedirect.com/science/article/pii/0037073869900104.

Collison, J., 1996. Alluvial sediments. In: Reading, H. (Ed.), Sedimentary Environments: Processes, Facies and Stratigraphy, third ed. Blackwell Publishing, 350 Main Street, Malden, MA 02148-5020, USA, pp. 37–81, chapter 3.

Custodio, E., Llamas, M., 1996. Hidrología SubterrÁnea. In: Geología y Geografía-Hidrología, (v. 2), Ed. Omega, URL https://books.google.cl/books?id=4ilVAAAACAAJ.

Dalla Santa, G., Galgaro, A., Sassi, R., Cultrera, M., Scotton, P., Mueller, J., Bertermann, D., Mendrinos, D., Pasquali, R., Perego, R., Pera, S., Di Sipio, E., Cassiani, G., De Carli, M., Bernardi, A., 2020. An updated ground thermal properties database for GSHP applications. Geothermics 85, 101758. http://dx.doi.org/10.1016/j.geothermics.2019.101758, URL https://www.sciencedirect.com/science/article/pii/S0375650519301944.

DGA, 1986. Mapa Hidrogeológico de Chile 1:2.500.000. Technical Report, Ministerio de Obras Públicas de Chile.

DGA, 2012. Estudio Cuencas Principales Región de Los Ríos. Technical Report, Ministerio de Obras Públicas de Chile.

DGA, 2013. Modelación Hidrogeológica Cuenca Estero Los Puercos, Región del Maule. Technical Report, Ministerio de Obras Públicas de Chile.

Fetter, C., 1999. Contaminant Hydrogeology, no. 301054892. Prentice-Hall, URL https://books.google.cl/books?id=4ilVAAAACAAJ.

Florides, G., Kalogirou, S., 2007. Ground heat exchangers—A review of systems, models and applications. Renew. Energy 32 (15), 2461–2478. http://dx.doi.org/10.1016/j.renene.2006.12.014, URL https://www.sciencedirect.com/science/article/pii/S0960148107000092.

Freeze, R., Cherry, J., 1979. Groundwater, Vol. 7632. Prentice-Hall Inc, Englewood Cliffs, NJ, p. 604.

Gizzi, M., Glenda, T., Cerino Abdin, E., Lo Russo, S., 2020. Thermally affected zone (TAZ) assessment in open-loop low-enthalpy groundwater heat pump systems (GWHPs): Potential of analytical solutions. Geofluids 2020, 1–13. http://dx.doi.org/10.1155/2020/2640917.

Halford, K., Kuniansky, E., 2002. Documentation of Spreadsheets for the Analysis of Aquifer-Test and Slug-Test Data. Technical Report, U.S. Geological Survey, Carson City, Nevada.

Hauser, A., 1995. Hoja Talca. Mapa 1: Talca (1de 2) Carta Hidrogeológica de Chile No. 2. Technical Report, Servicio Nacional de Geología y Minería.

Hildreth, W., Grunder, A., Drake, R., 1984. The Loma Seca Tuff and the Calabozos caldera: A major ash-flow and caldera complex in the southern Andes of central Chile. Geol. Soc. Am. Bull. - GEOL SOC AMER BULL 95, http://dx.doi.org/10.1130/0016-7606(1984)95<45:TLSTAT>2.0.CO;2.

Huang, S., Taniguchi, M., Yamano, M., ho Wang, C., 2009. Detecting urbanization effects on surface and subsurface thermal environment — A case study of Osaka. Sci. Total Environ. 407 (9), 3142–3152. http://dx.doi.org/10.1016/j.scitotenv.2008.04.019, Human Impacts on Urban Subsurface Environments, URL https://www.sciencedirect.com/science/article/pii/S0048969708004191.

Huneeus, N., A., U., Gayó, E., Osses, M., Arriagada, R., Valdés, M., Álamos, N., Amigo, C., Arrieta, D., Basoa, K., Billi, M., Blanco, G., 2020. El Aire Que Respiramos: Pasado, Presente Y Futuro. Technical Report, Centro de Ciencia del Clima y la Resiliencia (CR)2, Santiago.

IPCC, 2022. IPCC Sixth Assessment Report: Climate Change 2022, 28 F. ixth Assessment R, UN Environment.

Knight, M., 1975. Recent crevassing of the Erap river, Papua New Guinea. Aust. Geogr. Stud. 13, 77–84.

Lara, L., Moreno, H., Naranjo, J., Matthews, S., Pérez de Arce, C., 2006. Magmatic evolution of the Puyehue–Cordón Caulle volcanic complex (40°S), southern Andean volcanic zone: From shield to unusual rhyolitic fissure volcanism. J. Volcanol. Geotherm. Res. 157 (4), 343–366. http://dx.doi.org/10.1016/j.jvolgeores.2006.04.010, URL https://www.sciencedirect.com/science/article/pii/S0377027306001788.

Lee, J.-Y., Hahn, J.-S., 2006. Characterization of groundwater temperature obtained from the Korean national groundwater monitoring stations: Implications for heat pumps. J. Hydrol. 329 (3), 514–526. http://dx.doi.org/10.1016/j.jhydrol.2006.03.007, URL https://www.sciencedirect.com/science/article/pii/S0022169406001326.

Lo Russo, S., Taddia, G., Verda, V., 2012. Development of the thermally affected zone (TAZ) around a groundwater heat pump (GWHP) system: A sensitivity analysis. Geothermics 43, 66–74. http://dx.doi.org/10.1016/j.geothermics.2012.02.001, URL https://www.sciencedirect.com/science/article/pii/S0375650512000077.

Lund, J.W., Toth, A.N., 2021. Direct utilization of geothermal energy 2020 worldwide review. Geothermics 90, 101915. http://dx.doi.org/10.1016/j.geothermics.2020.101915, URL https://www.sciencedirect.com/science/article/pii/S0375650520302078.

Marcic, M., 2004. Long-term performance of central heat pumps in Slovenian homes. Energy Build. 36 (2), 185–193. http://dx.doi.org/10.1016/j.enbuild.2003.11.002, URL https://www.sciencedirect.com/science/article/pii/S0378778803001361.

Mella, M., Quiroz, D., 2010. Geología del Área Temuco-Nueva Imperial, Región de La Araucanía. 1 Mapa Escala 1:100.000. Technical Report vol. 122, Servicio Nacional de Geología y Minería, Carta Geológica de Chile, Serie Geología Básica, p. 46.

Metzger, T., Didierjean, S., Maillet, D., 2004. Optimal experimental estimation of thermal dispersion coefficients in porous media. Int. J. Heat Mass Transfer 47 (14), 3341–3353. http://dx.doi.org/10.1016/j.ijheatmasstransfer.2004.02.024, URL https://www.sciencedirect.com/science/article/pii/S0017931004000900.

Milenić, D., Vasiljević, P., Vranješ, A., 2010. Criteria for use of groundwater as renewable energy source in geothermal heat pump systems for building heating/cooling purposes. Energy Build. 42 (5), 649–657. http://dx.doi.org/10.1016/j.enbuild.2009.11.002, URL https://www.sciencedirect.com/science/article/pii/S0378778809002862.

Miller, J., 1996. Glacial sediments. In: Reading, H. (Ed.), Sedimentary Environments: Processes, Facies and Stratigraphy, third ed. Blackwell Publishing, 350 Main Street, Malden, MA 02148-5020, USA, pp. 454–483, chapter 11.

Morata, D., Aravena, D., Lahsen, A., Muñoz, M., Valdenegro, P., 2020. Chile up-date: The first south American geothermal power plant after one century of exploration. In: Proceedings World Geothermal Congress. Reykjavik, Iceland.

Morrone, B., Coppola, G., Raucci, V., 2014. Energy and economic savings using geothermal heat pumps in different climates. Energy Convers. Manage. 88, 189–198. http://dx.doi.org/10.1016/j.enconman.2014.08.007, URL https://www.sciencedirect.com/science/article/pii/S0196890414007316.

Mustafa Omer, A., 2008. Ground-source heat pumps systems and applications. Renew. Sustain. Energy Rev. 12 (2), 344–371. http://dx.doi.org/10.1016/j.rser.2006.10.003, URL https://www.sciencedirect.com/science/article/pii/S1364032106001249.

Perego, R., Pera, S., Bulgheroni, M., Dalla Santa, G., Galgaro, A., 2021. Thermal modeling of a Swiss urban aquifer and implications for geothermal heat pump systems. Hydrogeol. J. http://dx.doi.org/10.1007/s10040-021-02355-7.

Pérez, Y., Milovic, J., Troncoso, R., Hanisch, J., Helms, F., Toloczyki, M., 2003. Geología Para El Ordenamiento Territorial: Área De Osorno, Región De Los Lagos, Escala 1:100000. Technical Report, Servicio Nacional de Geología y Minería, Carta Geológica de Chile, Serie Geología Ambiental(6), 71.

Santibáñez Quezada, F., 2017a. Atlas agroclimático de Chile. Estado Actual Y Tendencias Del Clima. Tomo III: Regiones de Valparaíso, Metropolitana, O'Higgins y Maule. Technical Report, Universidad de Chile. Facultad de Ciencias Agronómicas: FIA.

Santibáñez Quezada, F., 2017b. Atlas agroclimático de Chile. Estado Actual Y Tendencias Del Clima. Tomo IV: Regiones del Biobío y de La Araucanía. Technical Report, Universidad de Chile. Facultad de Ciencias Agronómicas: FIA.

Santibáñez Quezada, F., 2017c. Atlas agroclimático de Chile. Estado Actual Y Tendencias Del Clima. Tomo V: Regiones de Los Ríos y Los Lagos. Technical Report, Universidad de Chile. Facultad de Ciencias Agronómicas: FIA.

Rubio, X., 1990. Estudio Geológico Regional y Estratigráfico de las Secuencias Terciarias de la Cuenca de Labranza, Temuco, IX Región. Taller de Título II (Inédito), Departamento de Geología y Geofísica, Universidad de Chile.

Sanner, B., Mands, E., Sauer, M.K., 2003. Larger geothermal heat pump plants in the central region of Germany. Geothermics 32 (4), 589–602. http://dx.doi.org/10.1016/j.geothermics.2003.07.010, Selected Papers from the European Geothermal Conference 2003, URL https://www.sciencedirect.com/science/article/pii/S0375650503000877.

Sarricolea, P., Herrera Ossandón, M., Meseguer-Ruiz, O., 2017. Climatic regionalisation of continental Chile. J. Maps 13, 66–73. http://dx.doi.org/10.1080/17445647.2016.1259592.

Smith, N.D., 1974. Sedimentology and bar formation in the Upper Kicking Horse River, a braided outwash stream. J. Geol. 82 (2), 205–223. http://dx.doi.org/10.1086/627959.

Smith, N.D., Smith, D.G., 1984. William River: An outstanding example of channel widening and braiding caused by bed-load addition. Geology 12 (2), 78–82. http://dx.doi.org/10.1130/0091-7613(1984)12<78:WRAOEO>2.0.CO;2.

Srivastava, R., Guzman-Guzman, A., 1998. Practical approximations of the well function. Groundwater 36 (5), 844–848. http://dx.doi.org/10.1111/j.1745-6584.1998.tb02203.x, URL https://ngwa.onlinelibrary.wiley.com/doi/abs/10.1111/j.1745-6584.1998.tb02203.x, arXiv:https://ngwa.onlinelibrary.wiley.com/doi/pdf/10.1111/j.1745-6584.1998.tb02203.x.

Varela, J., Moreno, H., 1982. Los depósitos de relleno de la depresión central de Chile entre los ríos lontué y bío-bío. In: III Congreso Geológico de Chile. pp. F280–F306.

Wu, Q., Xu, S., Zhou, W., LaMoreaux, J., 2015. Hydrogeology and design of groundwater heat pump systems. Environ. Earth Sci. 73 (7), 3683–3695. http://dx.doi.org/10.1007/s12665-014-3654-2.

Xu, M., Eckstein, Y., 1995. Use of weighted least-squares method in evaluation of the relationship between dispersivity and field scale. Ground Water 33, 905–908. http://dx.doi.org/10.1111/j.1745-6584.1995.tb00035.x.

Zhu, K., Blum, P., Ferguson, G., Balke, K.-D., Bayer, P., 2010. The geothermal potential of urban heat islands. Environ. Res. Lett. 5 (4), 044002. http://dx.doi.org/10.1088/1748-9326/5/4/044002.